Electronic Supplementary Information (ESI) for Dalton Transactions This journal is © The Royal Society of Chemistry 2018

Supporting Information For

A new quinoline based luminescent Zr(IV) metal-organic framework for the ultrasensitive recognition of 4-nitrophenol and Fe(III) ion

Chiranjib Gogoi and Shyam Biswas *

* To whom correspondence should be addressed. E-mail: sbiswas@iitg.ernet.in; Tel: 91-3612583309.

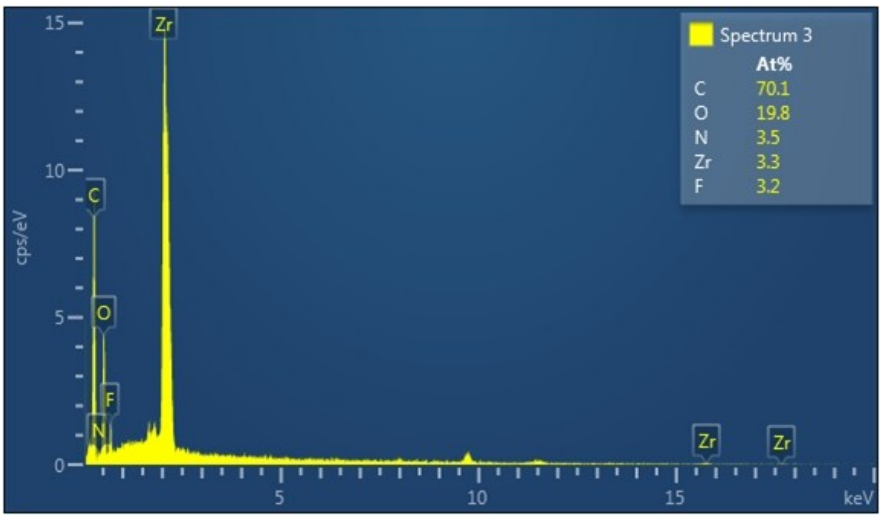

Figure S1. EDX spectrum of **1'**.

Table S1. Structural refinement parameters for **1** obtained from Rietveld refinement.

Formula of activated sample	$[Zr_6O_6(OH)_2(CF_3COO)_2(C_{11}H_5NO_4)_4(H_2O)_4]$
crystal system	Orthorhombic
space group	*Immm*
a / Å	11.673(2)
b / Å	17.688(3)
c / Å	25.498(3)
V/ Å^3	5264(1)
R_{wp} / %	6.1
R_p / %	4.7
R_{Bragg} / %	1.7
GoF	3.3

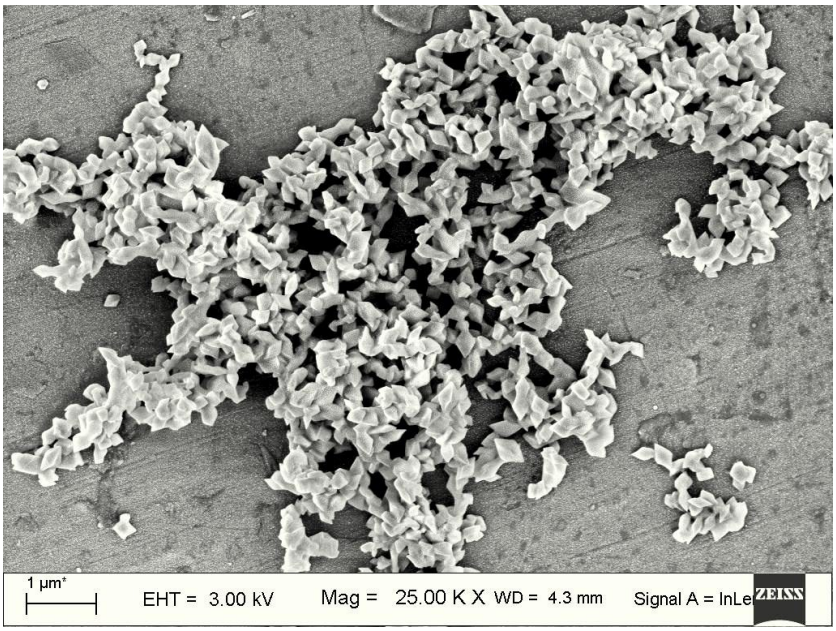

Figure S2. FE-SEM image of **1**.

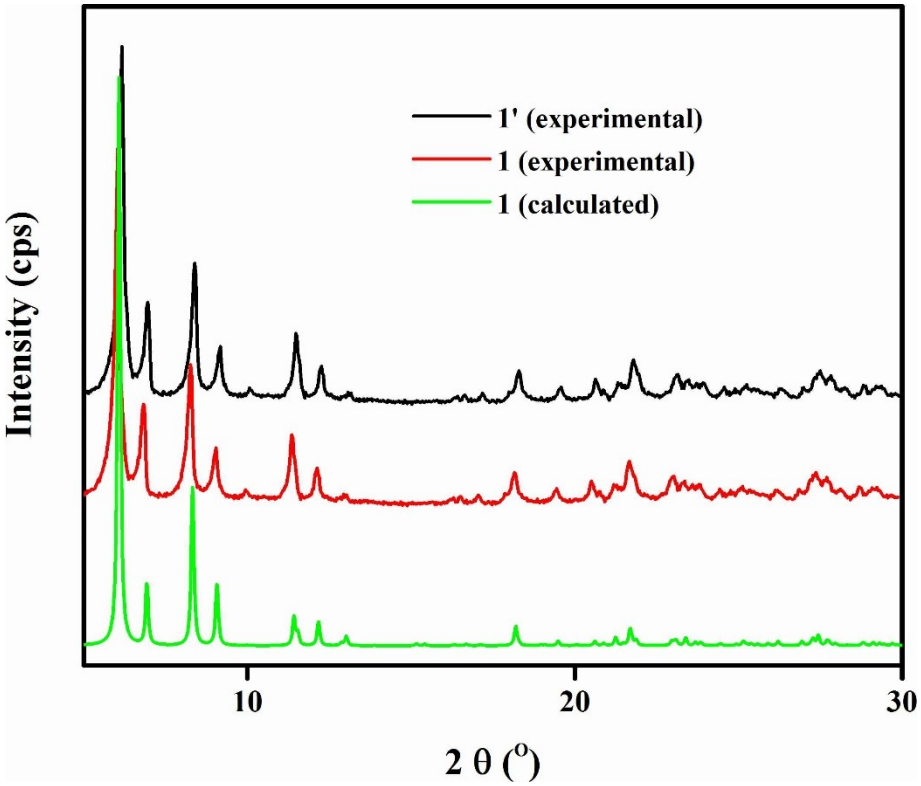

Figure S3. XRPD patterns of calculated **1**, as-synthesized **1** and thermally activated **1'**.

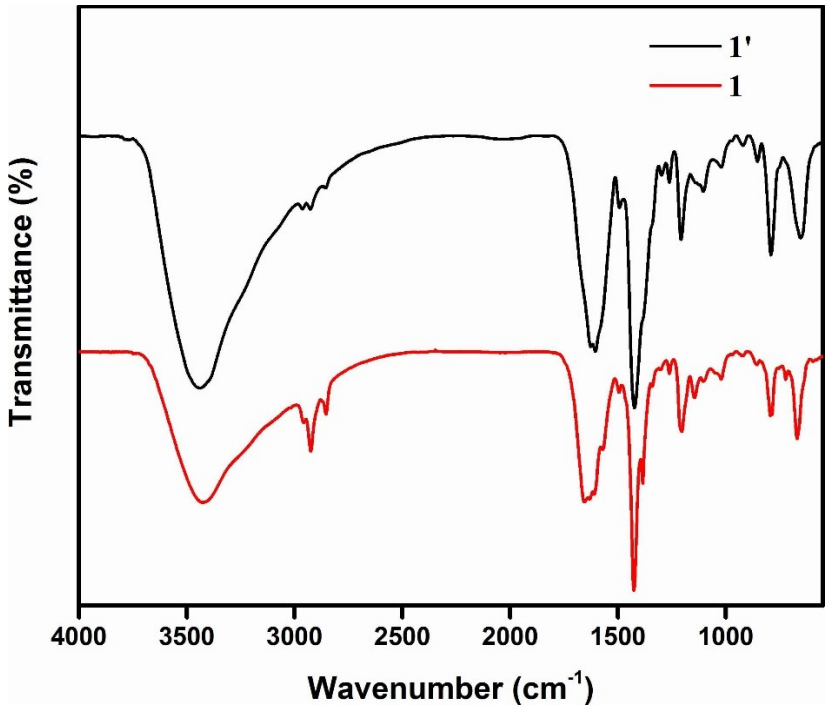

Figure S4. FT-IR spectra of **1** (red) and **1'** (black).

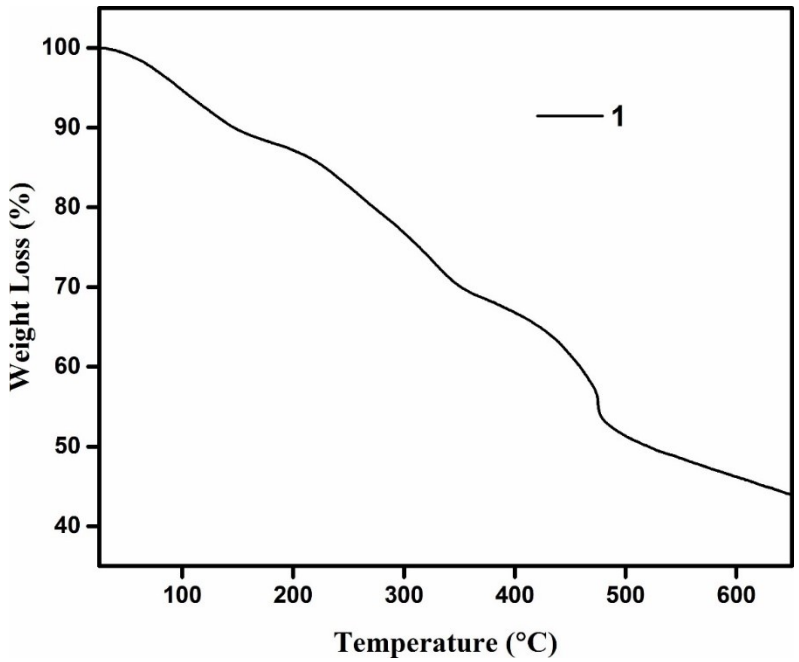

Figure S5. TG curve of as-synthesized **1** recorded in an argon atmosphere in the temperature range of 25-650 °C with a heating rate of 10 °C/min.

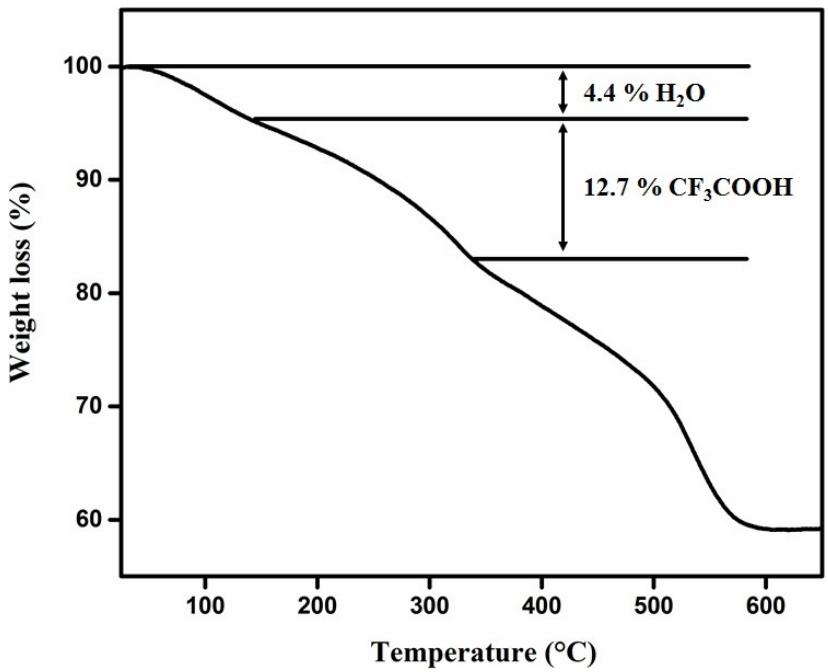

Figure S6. TG curve of activated **1'** recorded in an argon atmosphere in the temperature range of 25-650 °C with a heating rate of 10 °C/min.

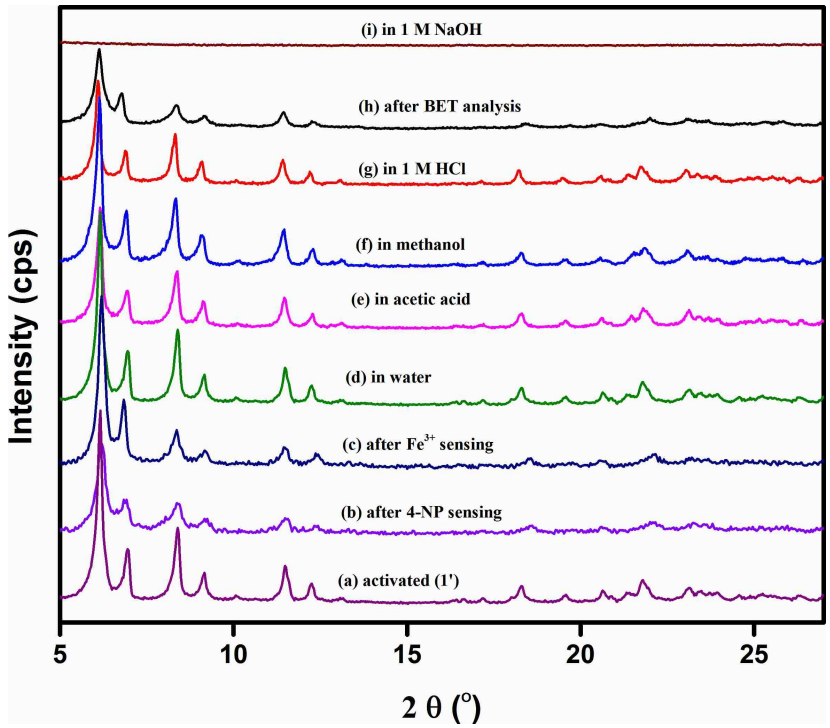

Figure S7. XRPD patterns of **1** in different forms: (a) activated; (b) after 5 cycles of fluorescence titration experiments with 4-NP; (c) after 5 cycles of fluorescence titration experiments with Fe^{3+} ions; (d) after treatment with water; (e) after treatment with acetic acid; (f) after treatment with methanol; (g) after treatment with 1(M) HCl; (h) after BET analysis; (i) after treatment with 1(M) NaOH.

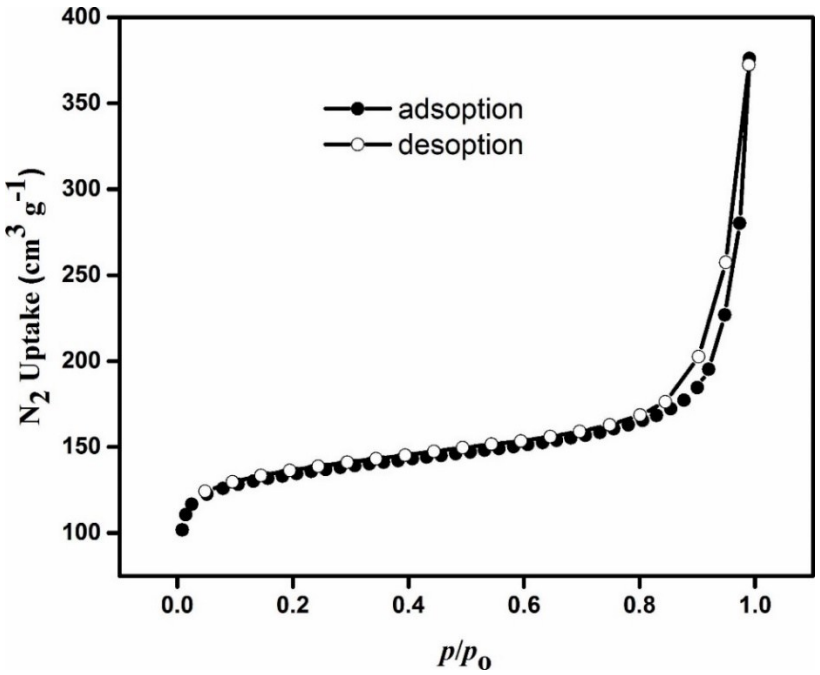

Figure S8. N_2 adsorption (filled circles) and desorption (empty circles) isotherms of thermally activated **1'** measured at –196 °C.

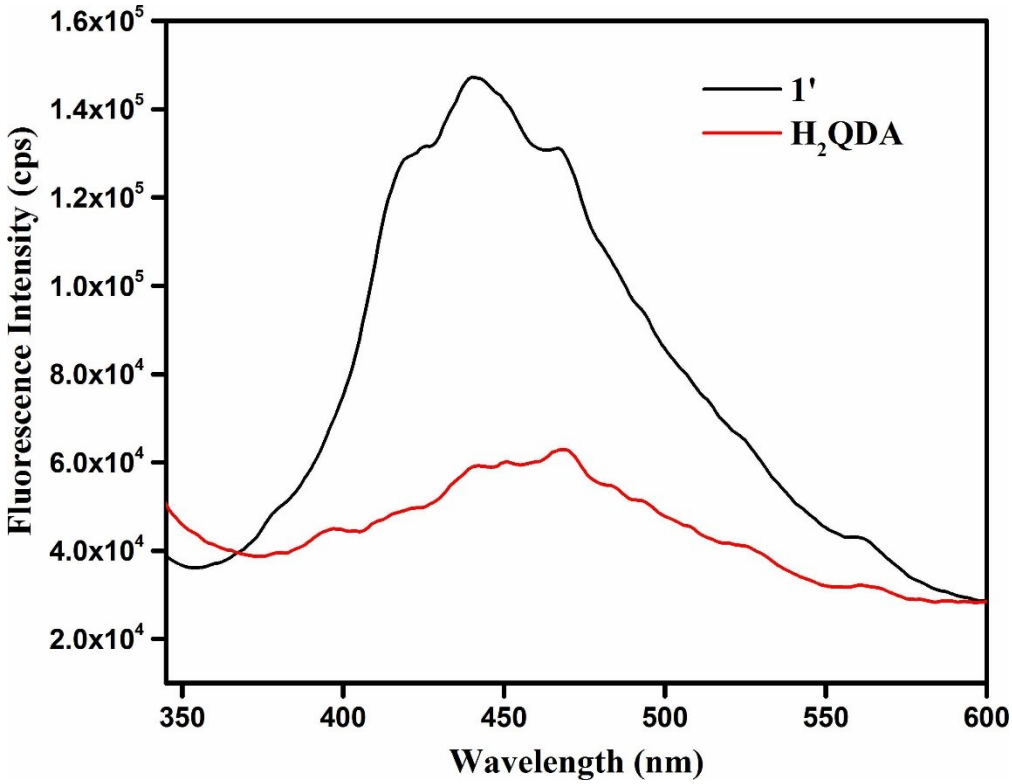

Figure S9. Emission spectra of H_2QDA ligand (red, λ_{ex} = 320 nm) and compound **1'** (black, λ_{ex} = 320 nm) measured in the solid state.

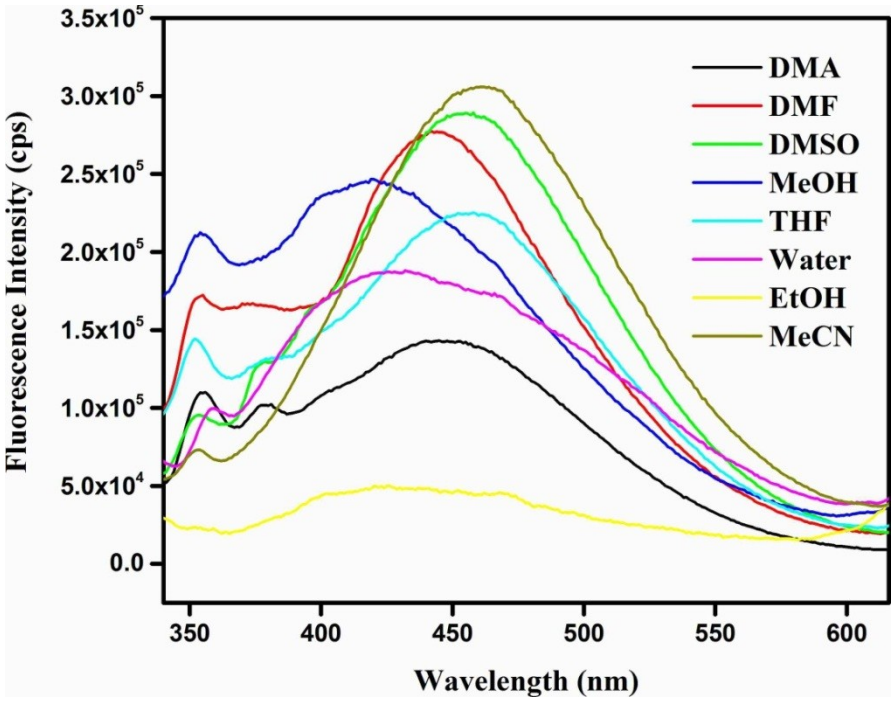

Figure S10. Fluorescence emission spectra of **1'** in common organic solvents (λ_{ex} = 320 nm).

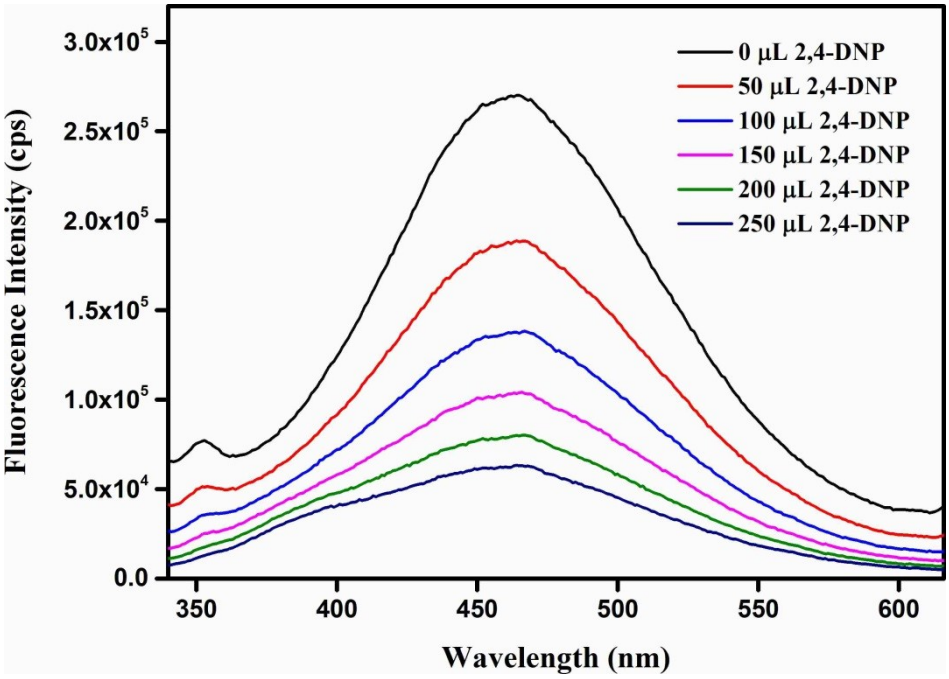

Figure S11. Quenching of the fluorescence intensity of **1'** by incremental addition of 3 mM 2,4-DNP solution to a 3 mL suspension of **1'** in acetonitrile.

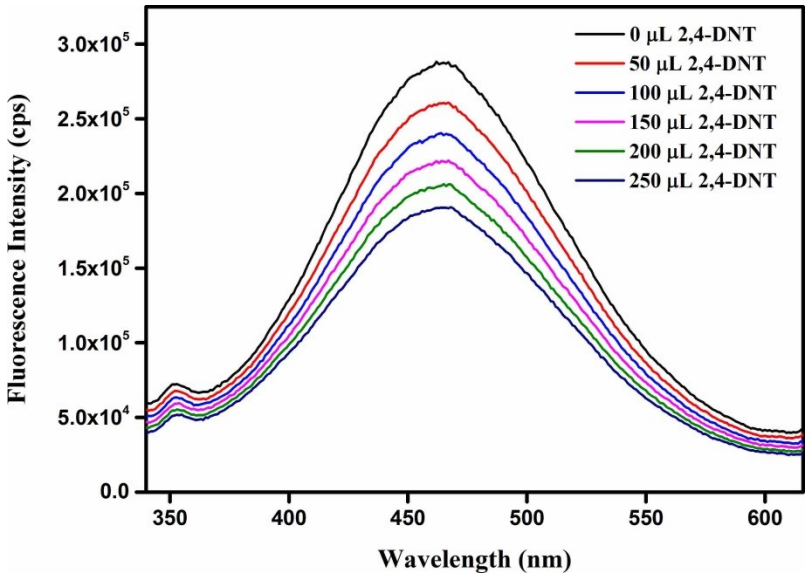

Figure S12. Quenching of fluorescence intensity of **1'** by incremental addition of 3 mM 2,4-DNT solution to a 3 mL suspension of **1'** in acetonitrile.

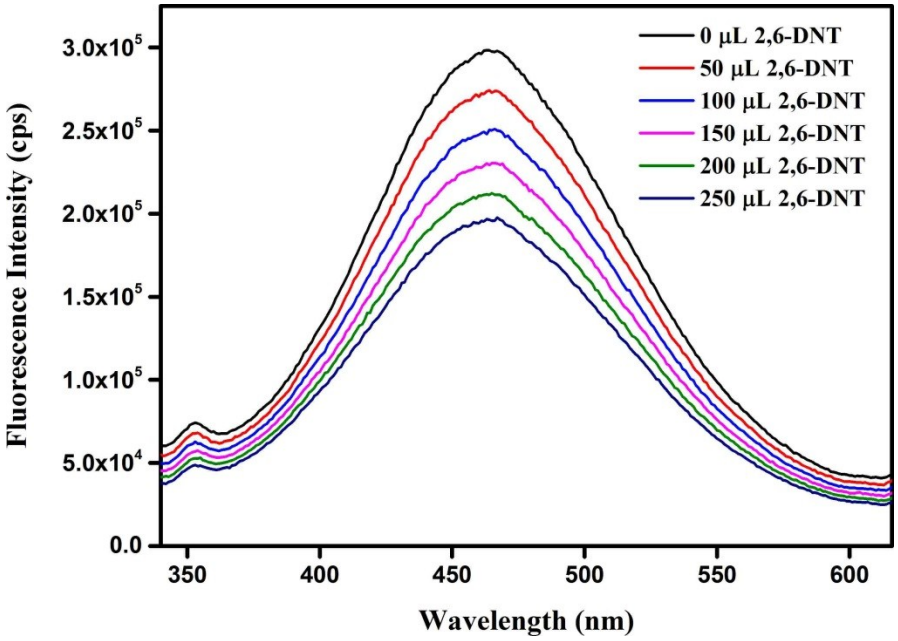

Figure S13. Quenching of fluorescence intensity of **1'** by incremental addition of 3 mM 2,6-DNT solution to a 3 mL suspension of **1'** in acetonitrile.

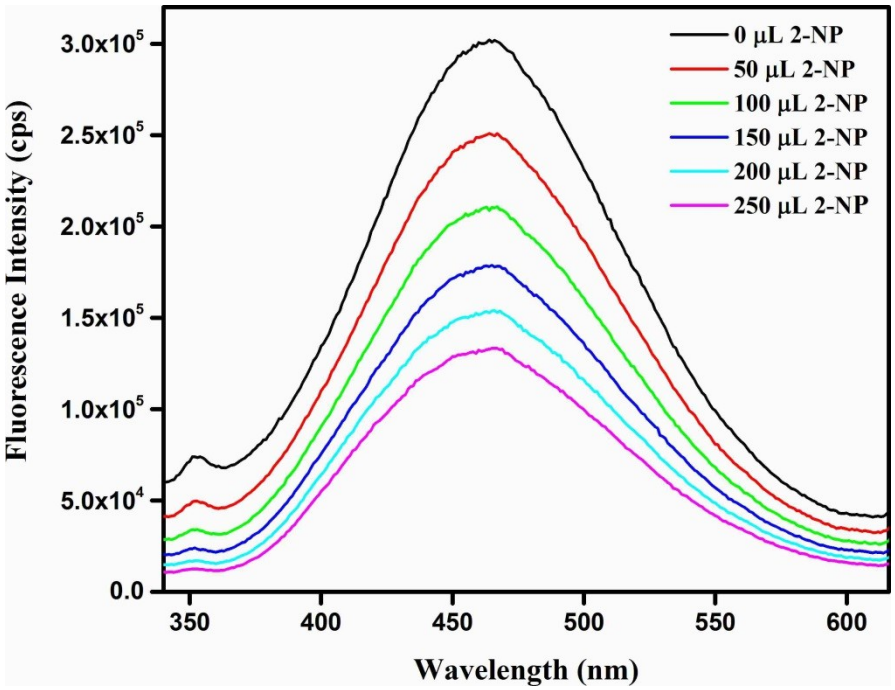

Figure S14. Quenching of fluorescence intensity of **1'** by incremental addition of 3 mM 2-NP solution to a 3 mL suspension of **1'** in acetonitrile.

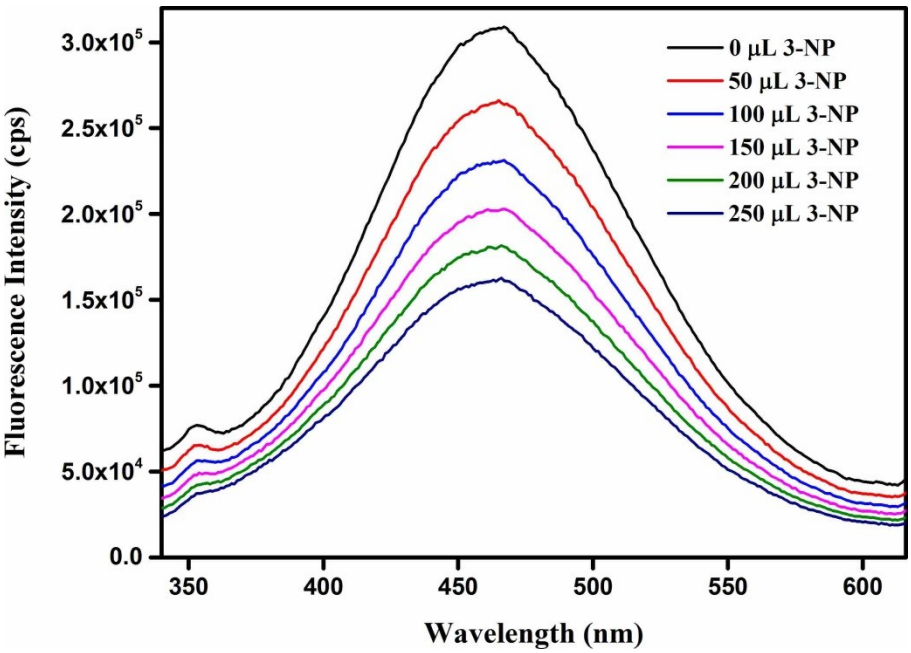

Figure S15. Quenching of fluorescence intensity of **1'** by incremental addition of 3 mM 3-NP solution to a 3 mL suspension of **1'** in acetonitrile.

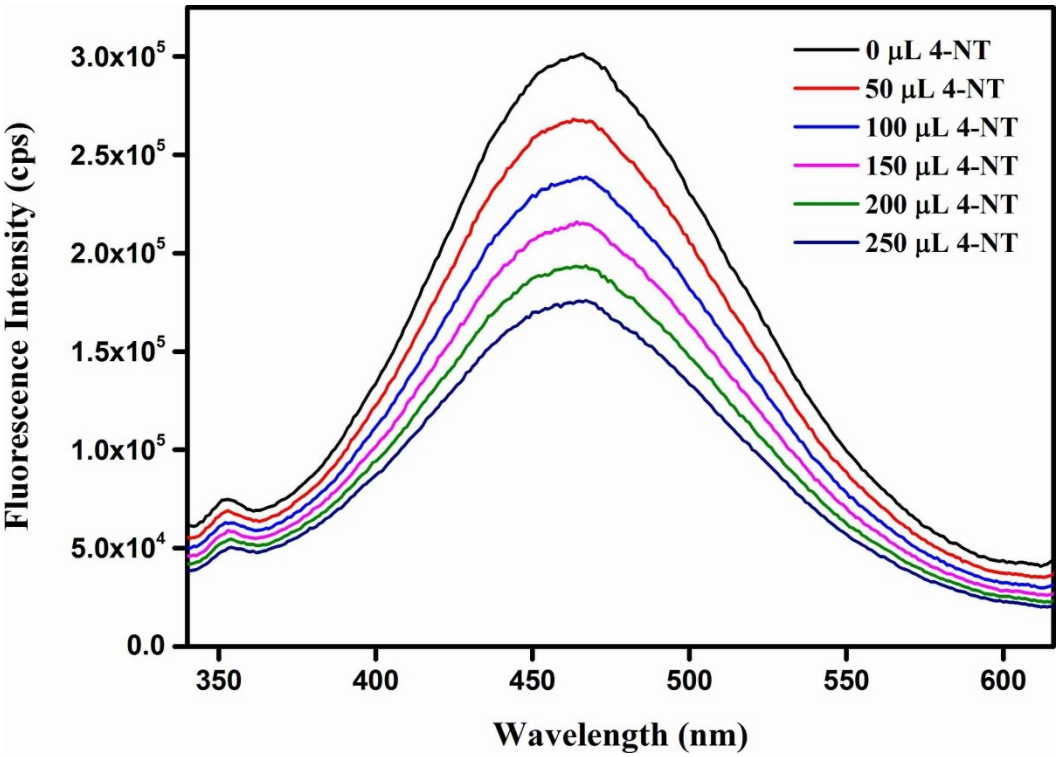

Figure S16. Quenching of fluorescence intensity of **1'** by incremental addition of 3 mM 4-NT solution to a 3 mL suspension of **1'** in acetonitrile.

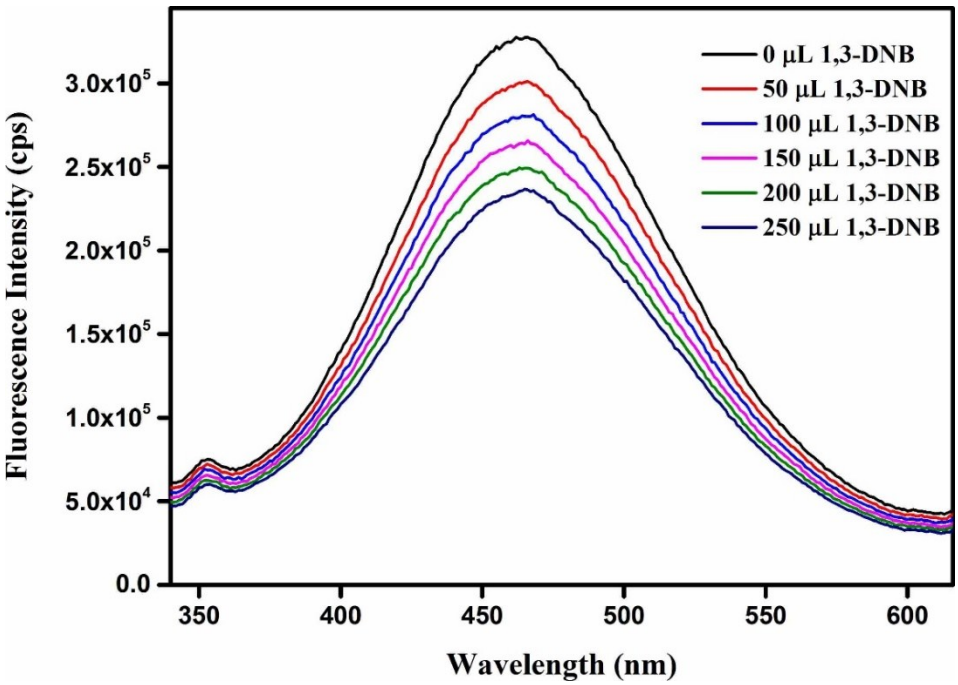

Figure S17. Quenching of fluorescence intensity of **1'** by incremental addition of 3 mM 1,3-DNB solution to a 3 mL suspension of **1'** in acetonitrile.

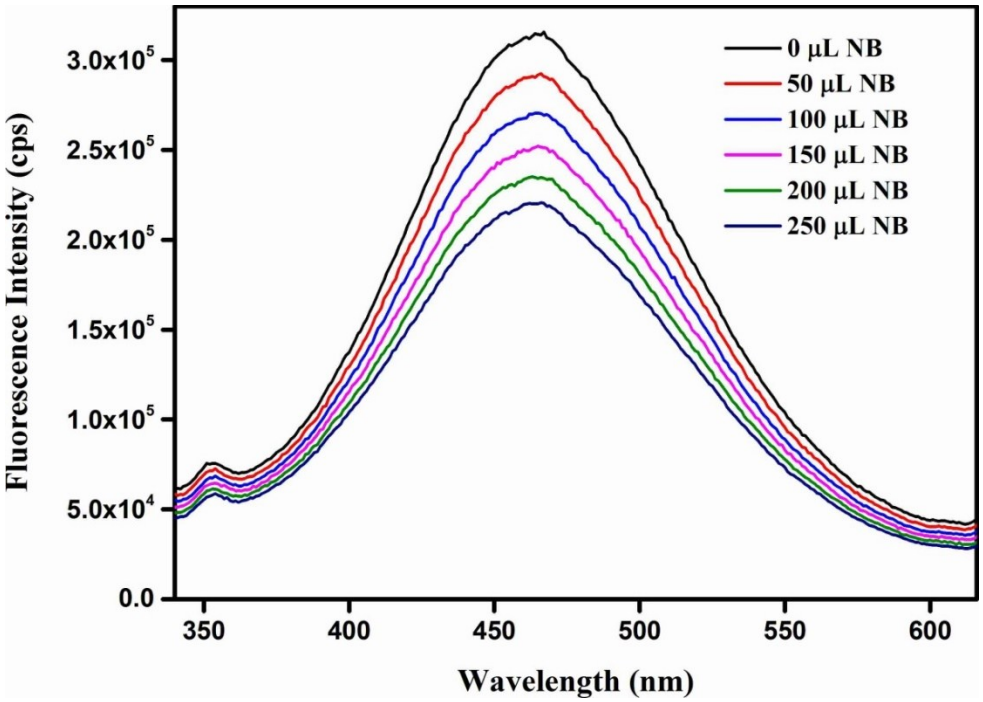

Figure S18. Quenching of fluorescence intensity of **1'** by incremental addition of 3 mM NB solution to a 3 mL suspension of **1'** in acetonitrile.

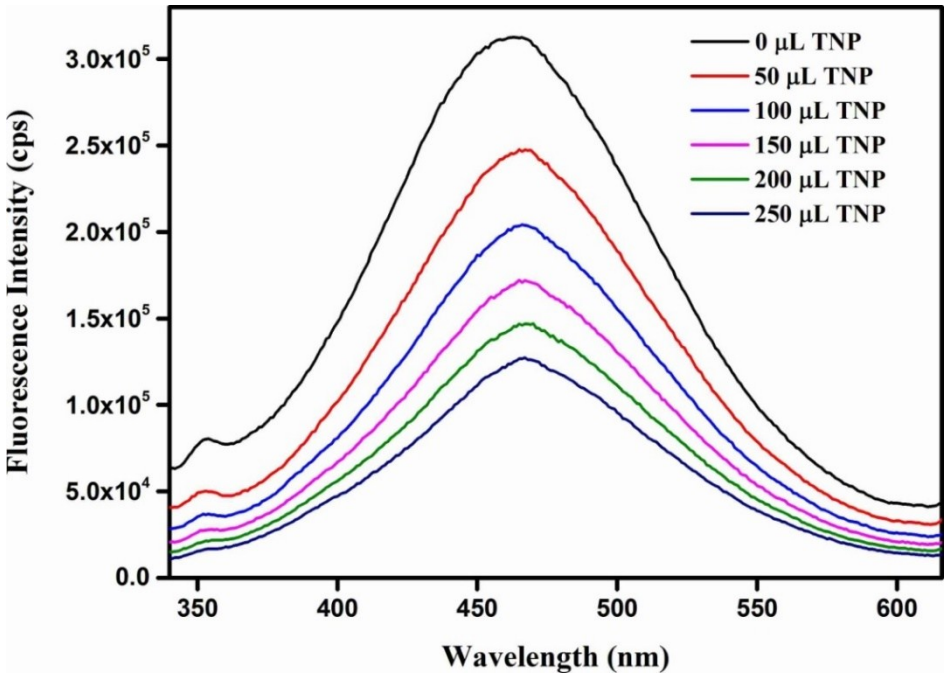

Figure S19. Quenching of fluorescence intensity of **1'** by incremental addition of 3 mM TNP solution to a 3 mL suspension of **1'** in acetonitrile.

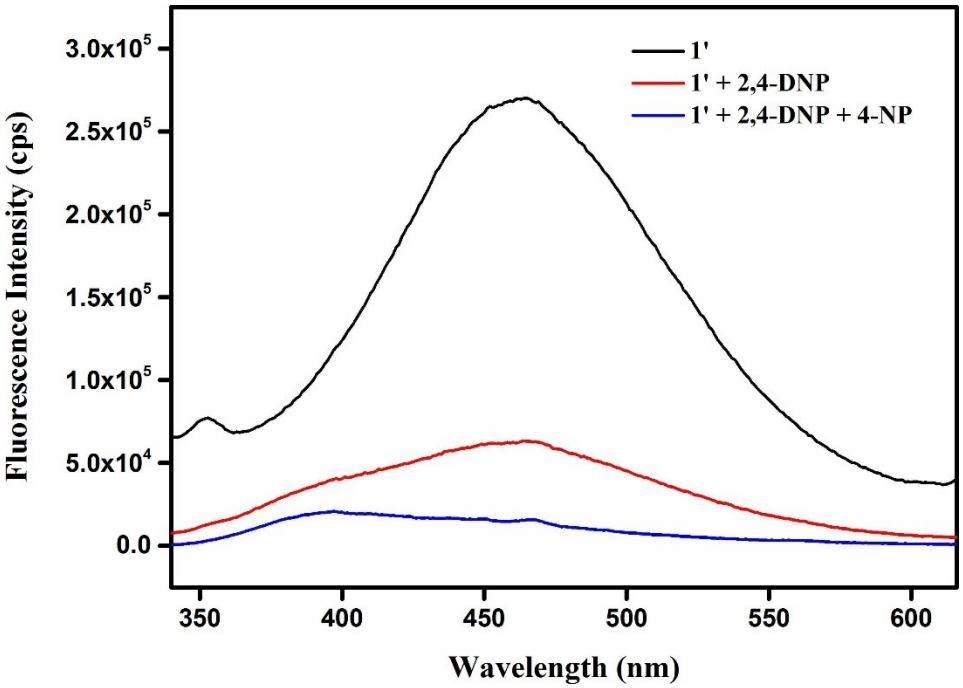

Figure S20. Change in the fluorescence intensity of **1′** upon addition of 3 mM 2,4-DNP solution (250 μL) in presence of 3 mM 4-NP (250 μL) solution.

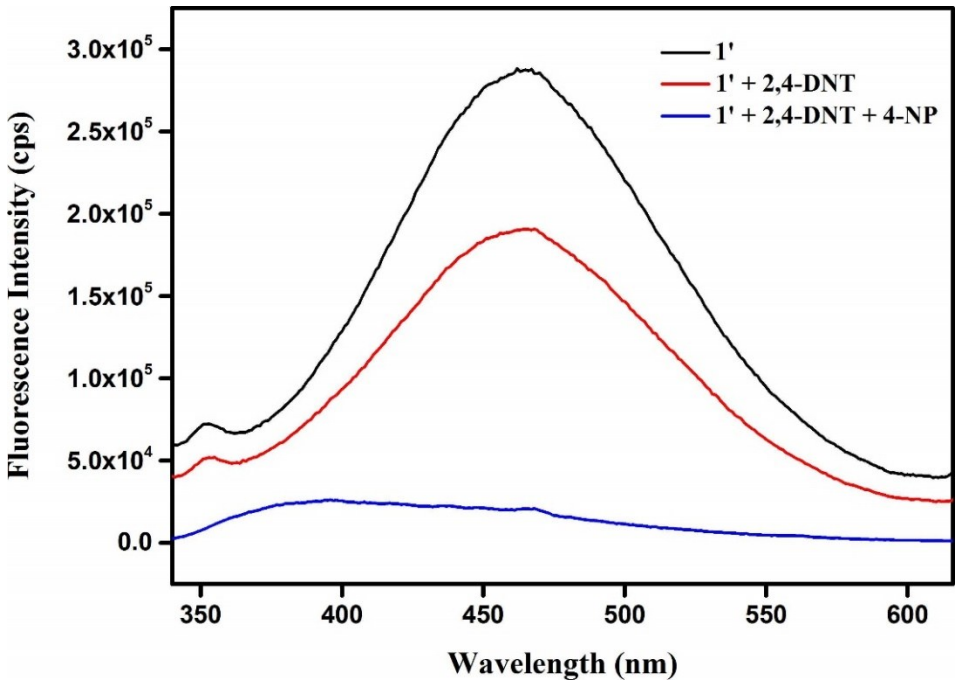

Figure S21. Change in the fluorescence intensity of **1′** upon addition of 3 mM 2,4-DNT solution (250 μL) in presence of 3 mM 4-NP (250 μL) solution.

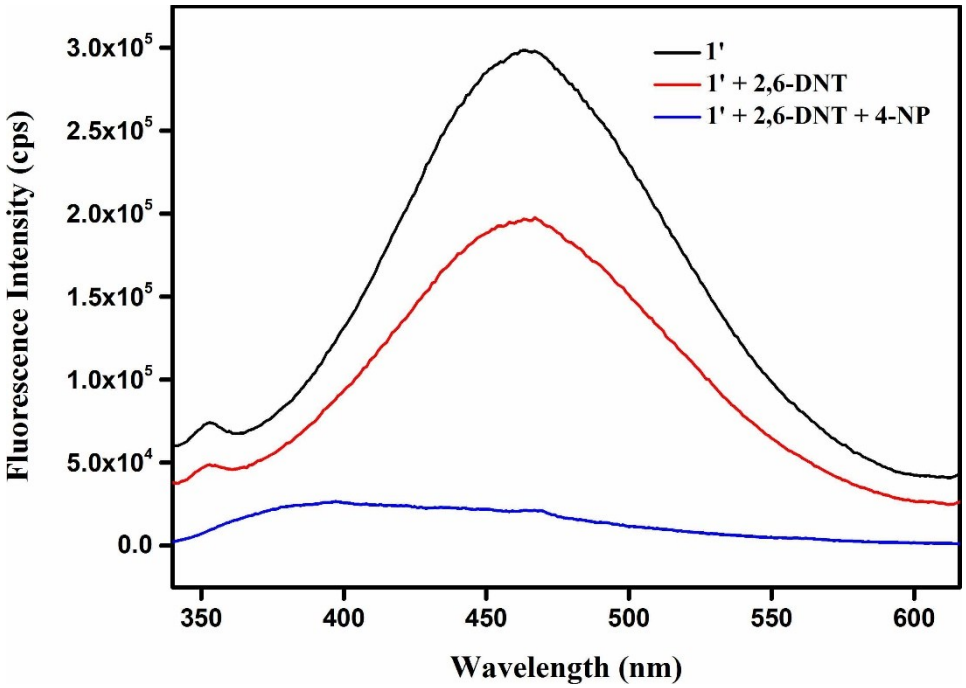

Figure S22. Change in the fluorescence intensity of **1′** upon addition of 3 mM 2,6-DNT solution (250 μL) in presence of 3 mM 4-NP (250 μL) solution.

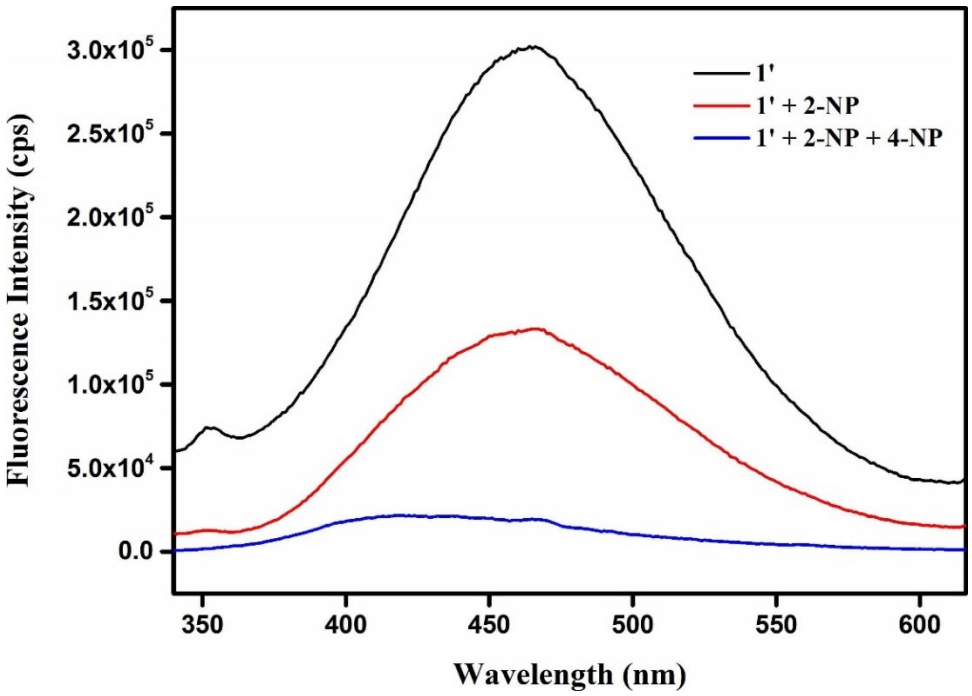

Figure S23. Change in the fluorescence intensity of **1′** upon addition of 3 mM 2-NP solution (250 μL) in presence of 3 mM 4-NP (250 μL) solution.

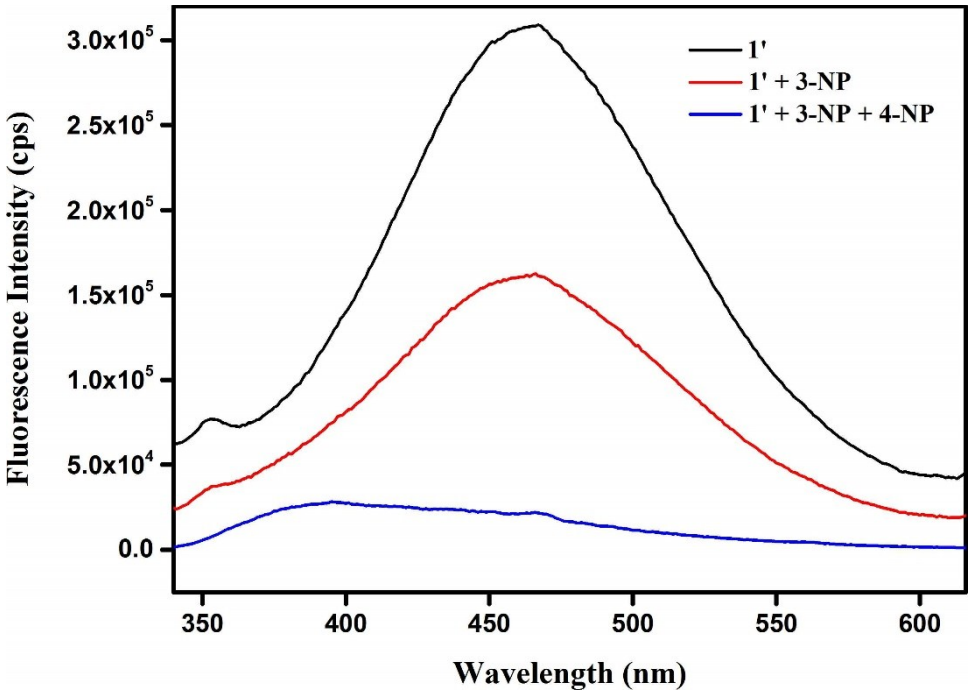

Figure S24. Change in the fluorescence intensity of **1′** upon addition of 3 mM 3-NP solution (250 μL) in presence of 3 mM 4-NP (250 μL) solution.

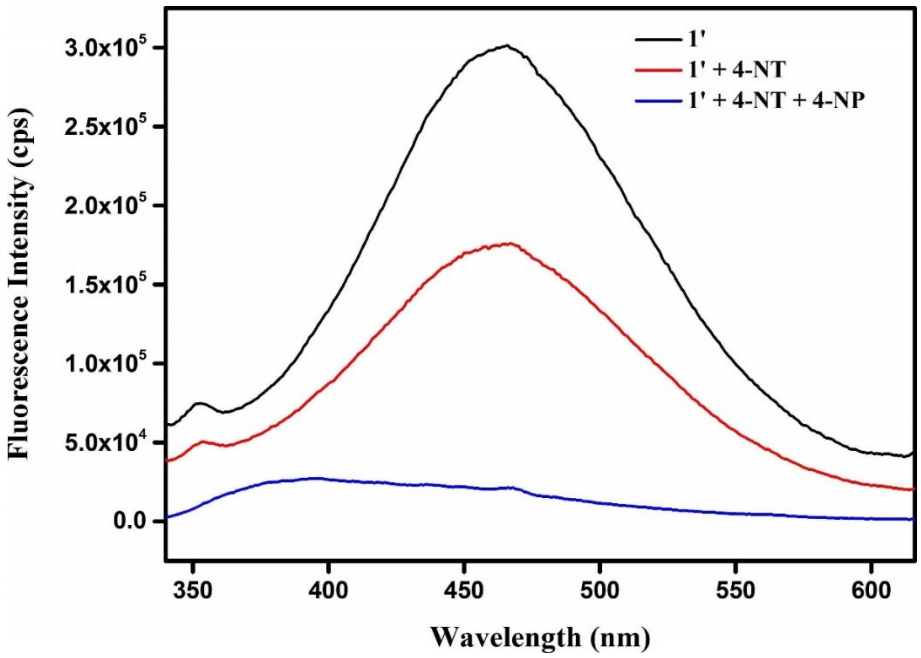

Figure S25. Change in the fluorescence intensity of **1′** upon addition of 3 mM 4-NT solution (250 μL) in presence of 3 mM 4-NP (250 μL) solution.

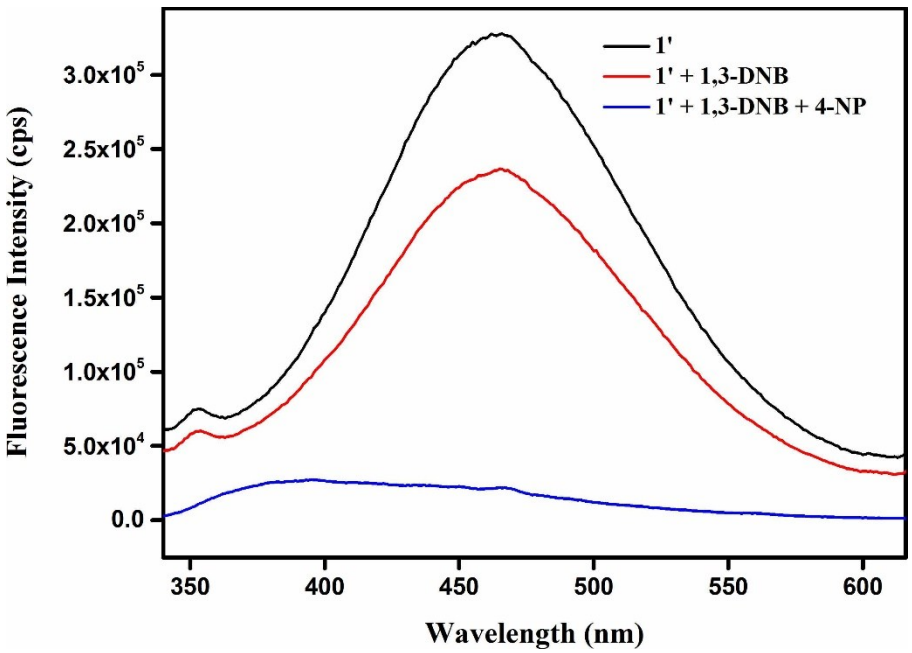

Figure S26. Change in the fluorescence intensity of **1′** upon addition of 3 mM 1,3-DNB solution (250 μL) in presence of 3 mM 4-NP (250 μL) solution.

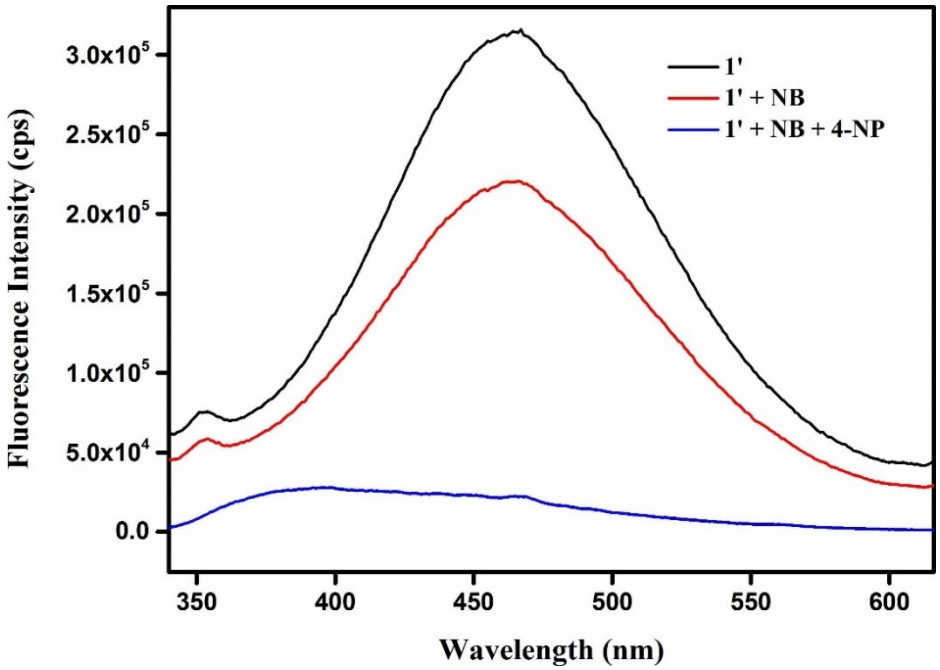

Figure S27. Change in the fluorescence intensity of **1′** upon addition of 3 mM NB solution (250 μL) in presence of 3 mM 4-NP (250 μL) solution.

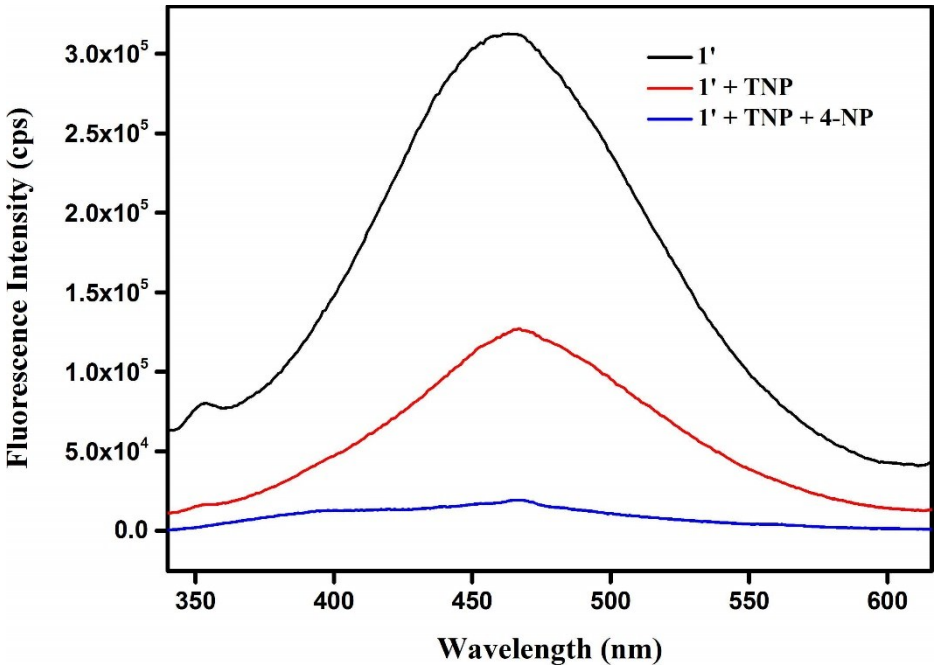

Figure S28. Change in the fluorescence intensity of **1′** upon addition of 3 mM TNP solution (250 μL) in presence of 3 mM 4-NP (250 μL) solution.

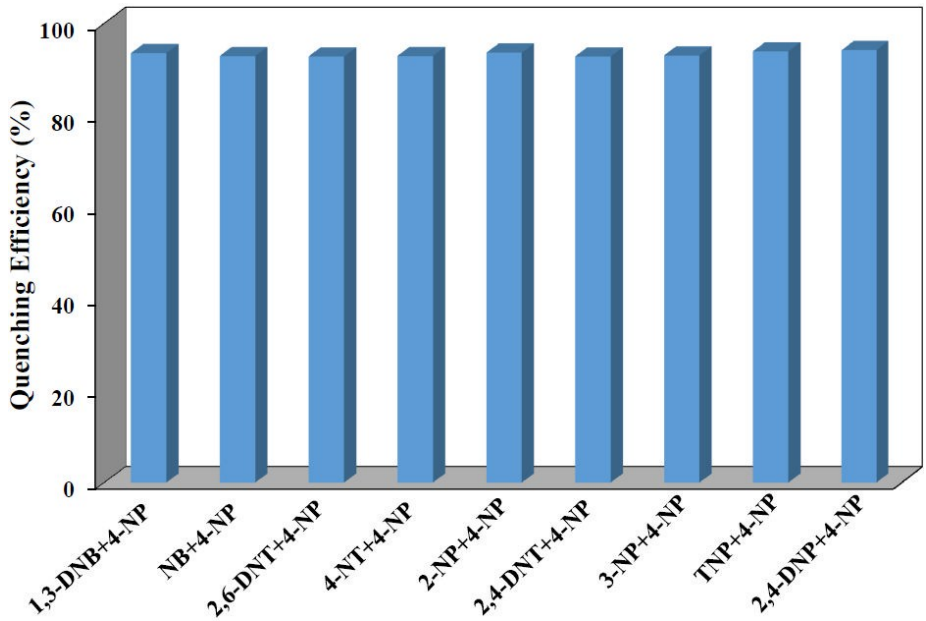

Figure S29. Effect of other NAEs on the quenching efficiency of 4-NP.

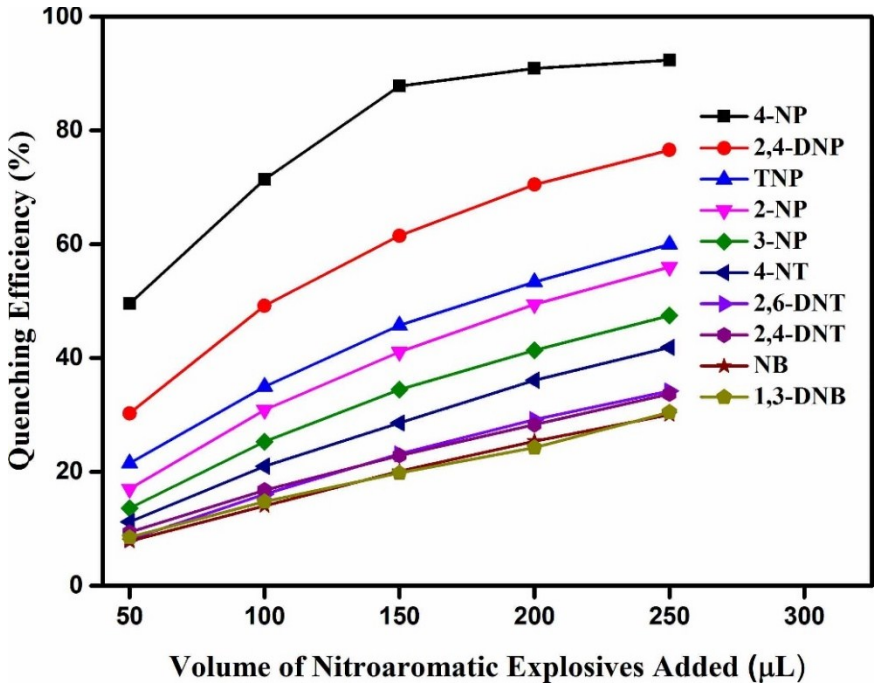

Figure S30. Change of the fluorescence quenching efficiencies upon gradual addition of 3 mM solution of various nitroaromatic explosives to a 3 mL well-dispersed suspension of **1′** in acetonitrile.

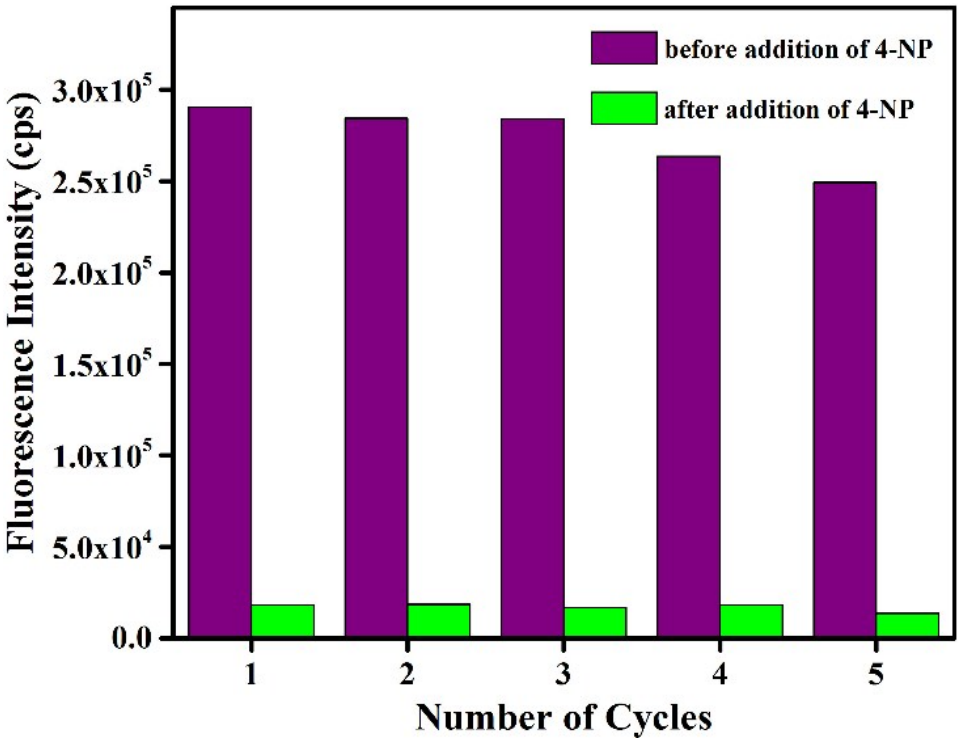

Figure S31. Recyclability test for the detection of 4-NP by **1'**.

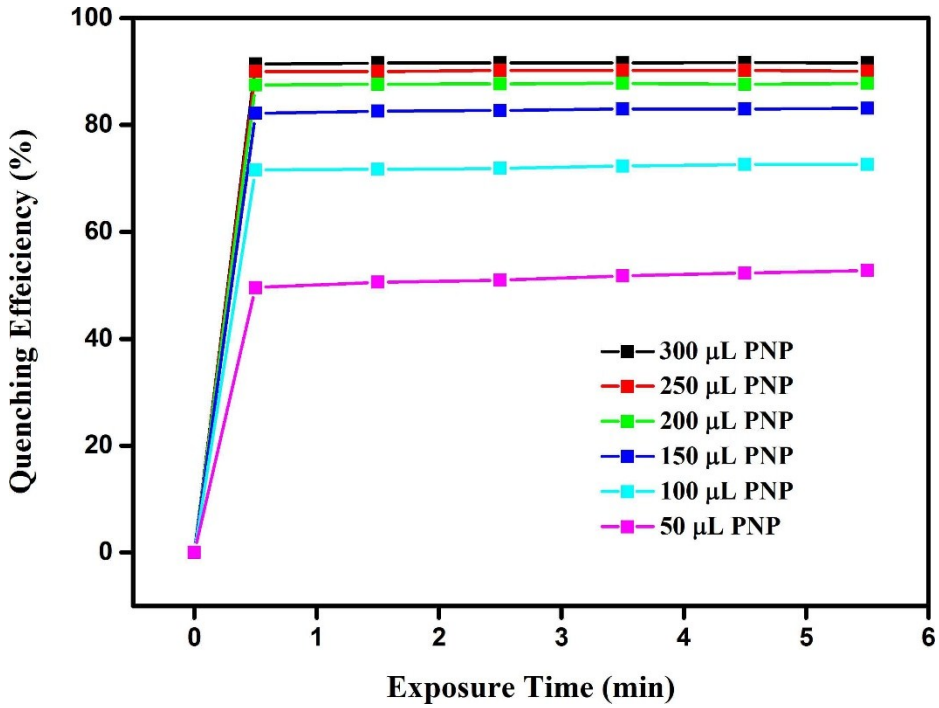

Figure S32. Quenching efficiencies of **1'**as a function of exposure time.

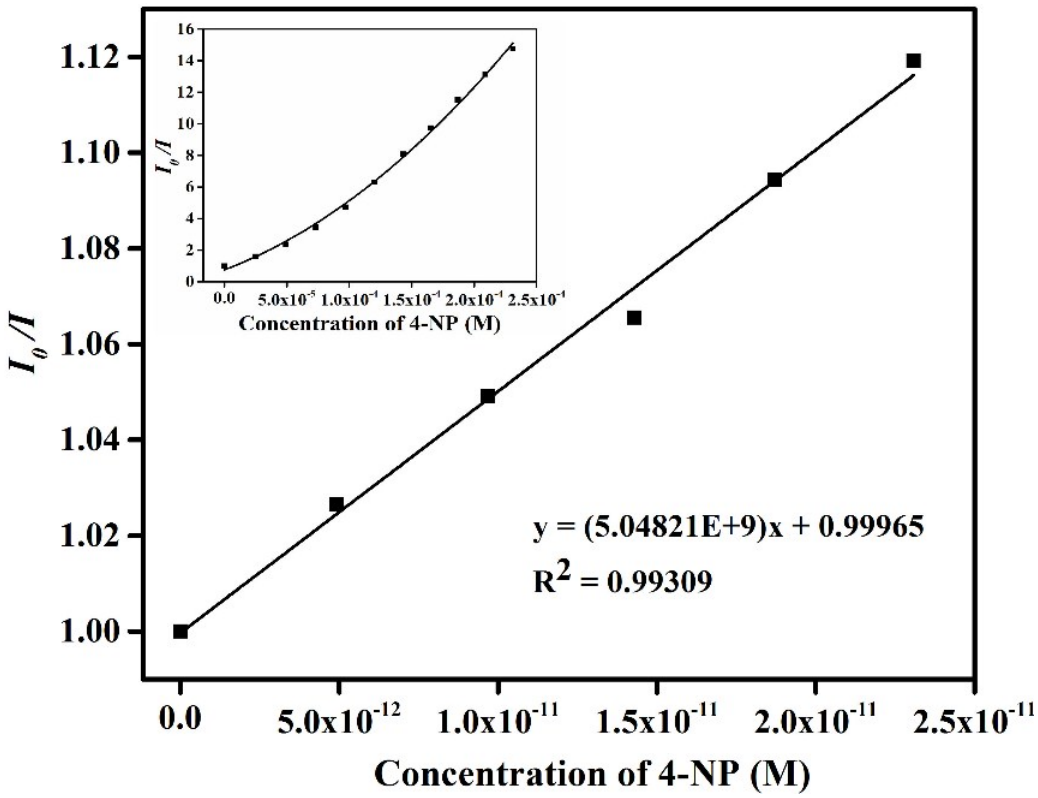

Figure S33. Stern-Volmer plot for the quenching of **1'** at lower concentrations of 4-NP. Inset: non-linearity of the Stern-Volmer plot at higher concentrations of 4-NP.

Table S2. A comparison of the Stern-Volmer constant (K_{sv}), detection limit and medium used for the detection of 4-NP by luminescent MOFs reported till date.

Sl. No.	MOF	K_{sv} (M^{-1})	Detection Limit	Medium Used	Ref.
1	$Zr_6O_4(OH)_4(CF_3COO)_4(C_{11}H_5NO_4)_4]\cdot 10H_2O\cdot 3DMF$	5.04×10^{9}	1.01×10^{-11} M	acetonitrile	This work
2	$[Zr_6O_4(OH)_4(2,7\text{-}CDC)_6]\cdot 19H_2O\cdot 2DMF$	1.40×10^{4}	1.80×10^{-8} M	THF	1
3	$[Cu_3(L)_{1.5}(H_2O)_3]\cdot 3DEF\cdot 20H_2O$ (UPC-21)	3.10×10^{6}	89.6 ppb	DMSO	2
4	$Ba_5(ADDA)_5(EtOH)_2(H_2O)_3\cdot 5DMF$ (UPC-17)	6.4×10^{3}	2.27×10^{-7} M	MeOH	3
		8.9×10^{3}	2.19×10^{-7} M	acetone	
		1.26×10^{4}	1.57×10^{-7} M	THF	
4	$[Eu_2(L)_2(H_2O)_3]\cdot 2H_2O$	2.20×10^{4}	-	DMSO	4
5	$[Zr_6O_4(OH)_8(H_2O)_4(CTTA)_{8/3}]$ (BUT-12)	4.20×10^{4}	-	water	5
6	$[Zr_6O_4(OH)_8(H_2O)_4(TTNA)_{8/3}]$ (BUT-13)	4.70×10^{4}	-	water	
7	$[Gd_6(L)_3(HL)_2(H_2O)_{10}]\cdot 18H_2O\cdot x(solvent)$	0.84×10^{4}	1.67 ppm	water	6
8	$[Eu_6(L)_3(HL)_2(H_2O)_{10}]\cdot 10H_2O\cdot x(solvent)$	-	1.7×10^{-6} M	water	7
9	$[Cd_4(bptc)_2(DMA)_4(H_2O)_2\cdot 4DMA]$	1.67×10^{5}	0.37 ppm	DMF	8

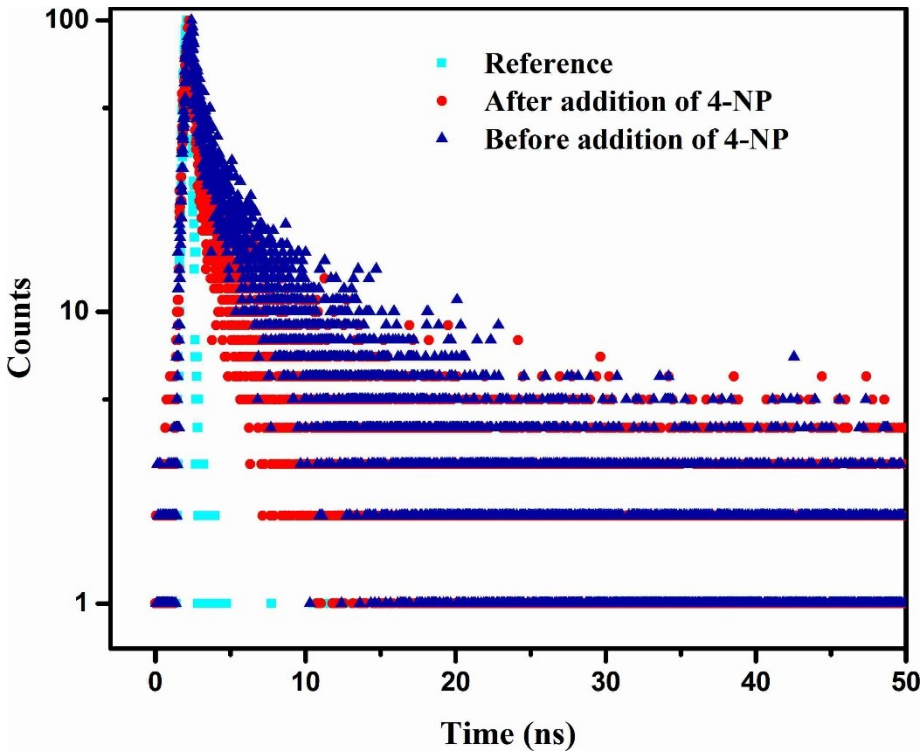

Figure S34. Lifetime decay profile of **1′** before and after addition of 300 μL of 3 mM 4-NP solution.

Table S3. Average excited-state lifetime (<τ>) values of **1'** before and after addition of 200 μL of 3 mM 4-NP solution (λ_{ex} = 330 nm).

Volume of PNP added (μL)	B_1	B_2	a_1	a_2	τ_1 (ns)	τ_2 (ns)	<τ>* (ns)	χ^2
0	0.023	0.006	0.36	0.64	0.87	6.30	4.36	1.00
200	0.030	0.004	0.41	0.59	0.46	5.28	3.29	1.00

* $\langle\tau\rangle = a_1\tau_1 + a_2\tau_2$

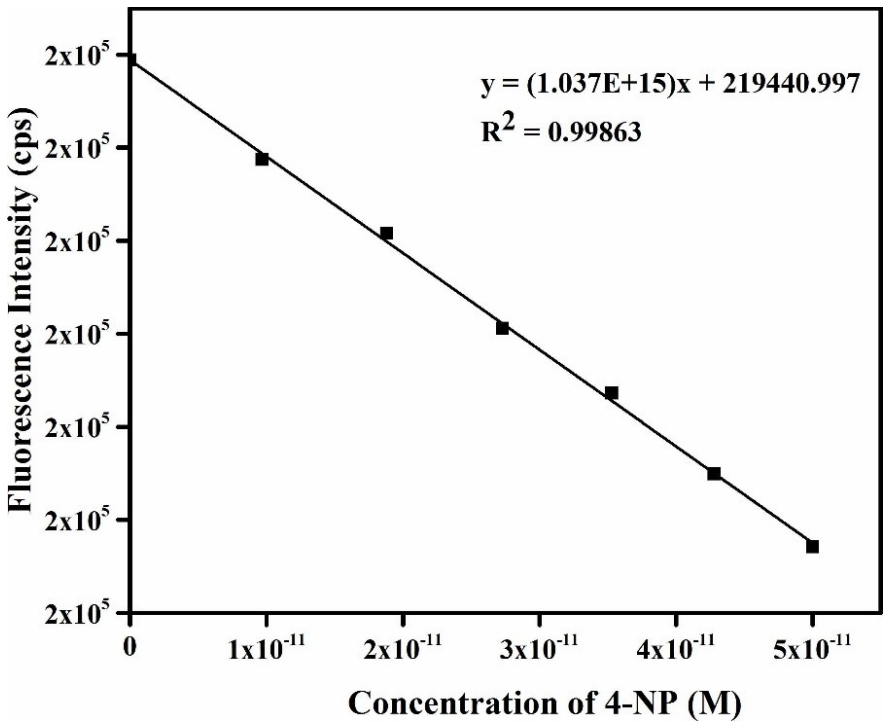

Figure S35. Fluorescence intensity of **1'** in acetonitrile as a function of 4-NP concentration.

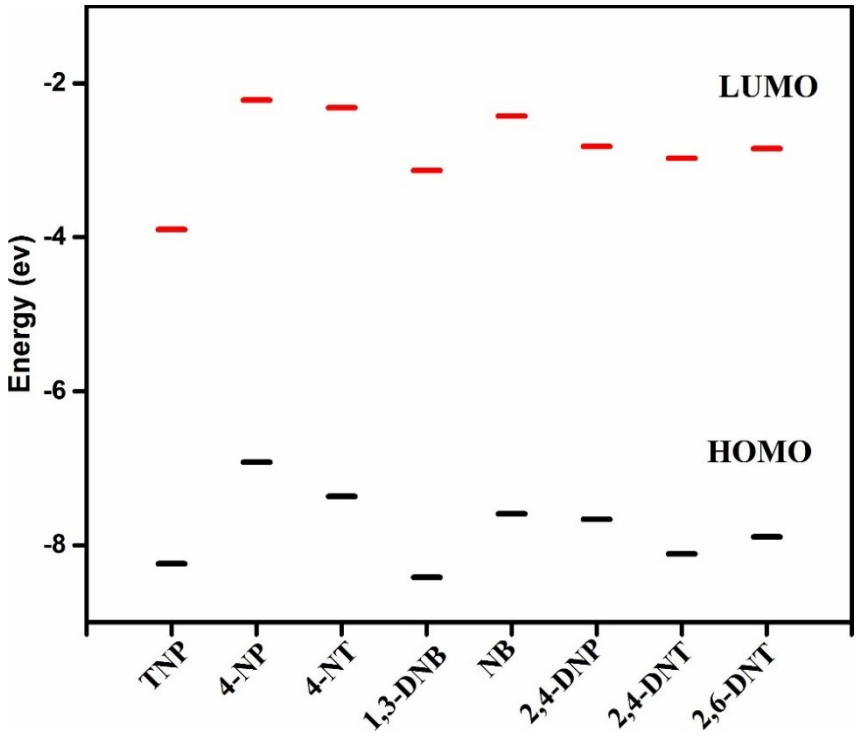

Figure S36. HOMO and LUMO energies for the nitroaromatic explosives.

Table S4. HOMO and LUMO energy levels of selected analytes calculated by density functional theory (DFT) at B3LYP/6-31G* accuracy level using Gaussian 09 package of program.[22]

Analytes	HOMO (eV)	LUMO (eV)	Band Gap (eV)
TNP	-8.2374	-3.898	4.3394
2,4-DNP	-7.6644	-2.8202	4.8442
4-NP	-6.9207	-2.2213	4.6994
4-NT	-7.3626	-2.3171	5.0455
2,4-DNT	-8.1131	-2.9769	5.1362
2,6-DNT	-7.8913	-2.8501	5.0412
1,3-DNB	-8.4129	-3.135	5.2779
NB	-7.5917	-2.4294	5.1623

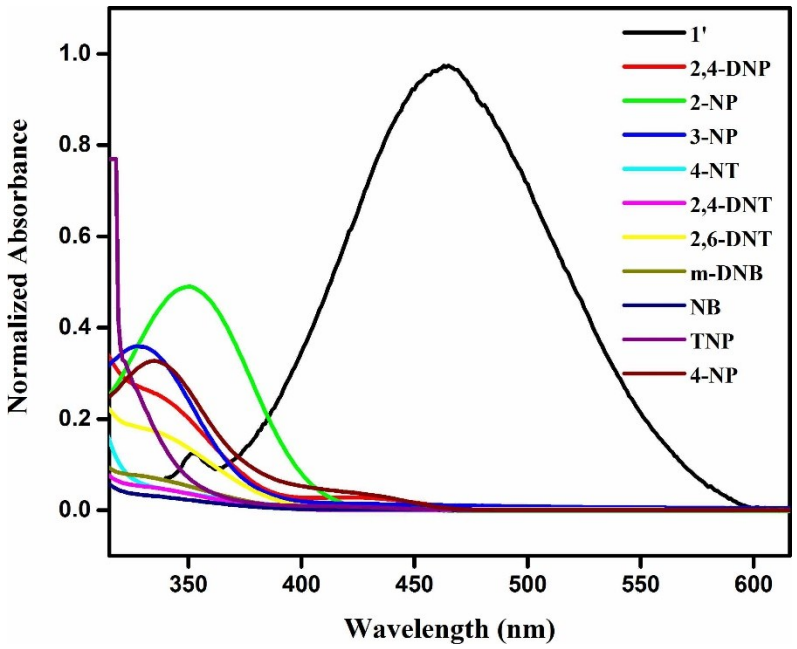

Figure S37. Overlap between the absorption spectra of the nitroaromatic explosives and the emission spectrum of the acetonitrile suspension of **1′**.

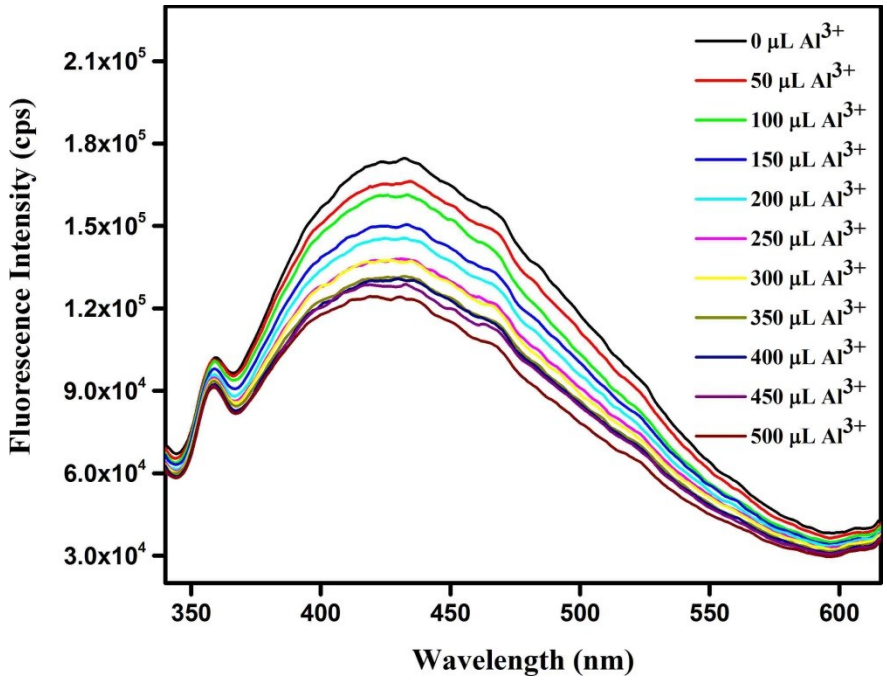

Figure S38. Change in the fluorescence intensity of **1′** upon incremental addition of 10 mM Al^{3+} solution in water.

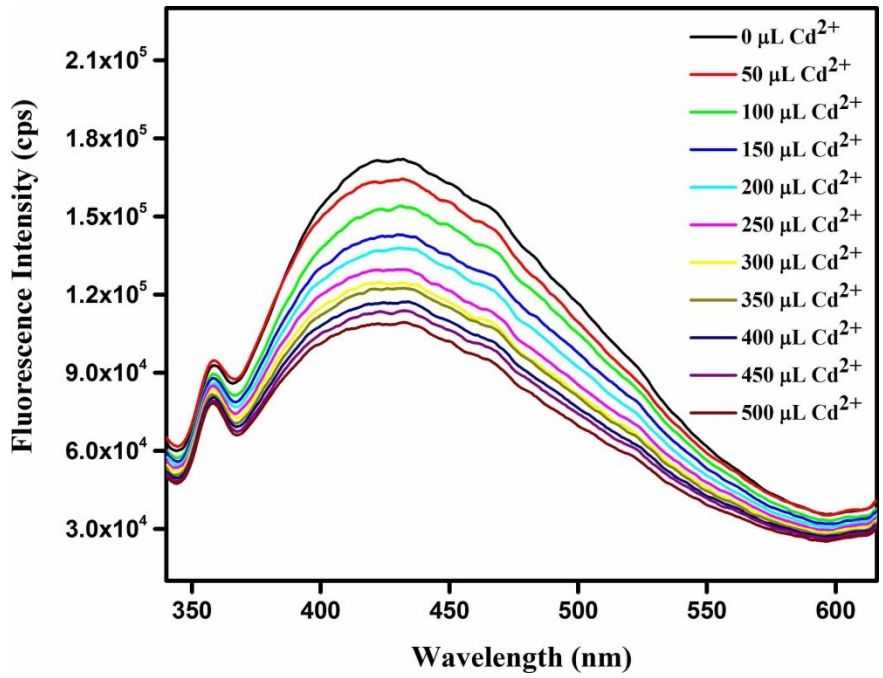

Figure S39. Change in the fluorescence intensity of **1′** upon incremental addition of 10 mM Cd^{2+} solution in water.

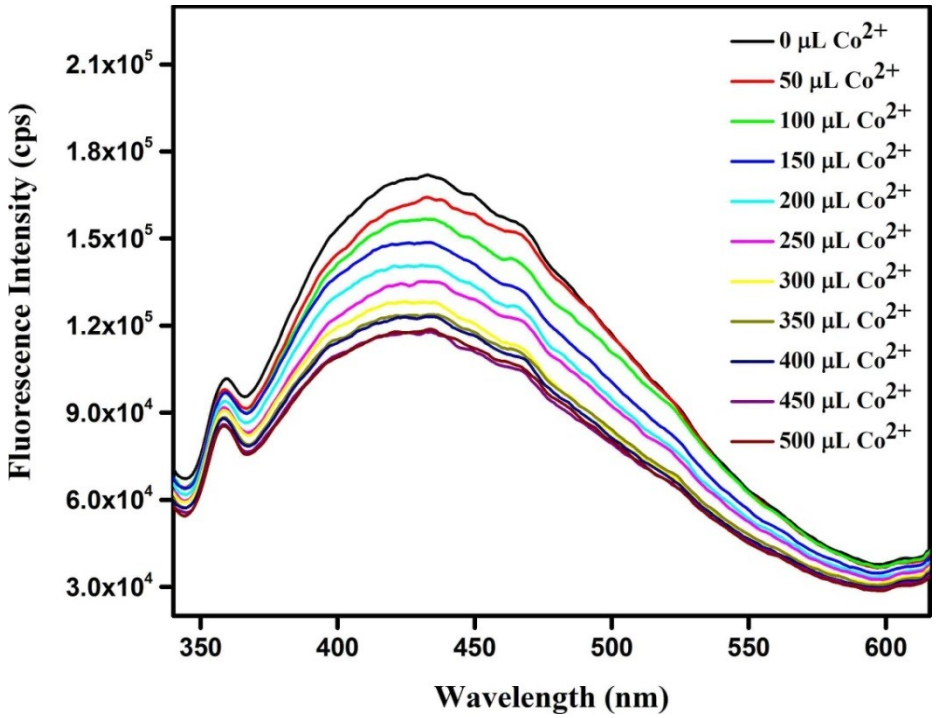

Figure S40. Change in the fluorescence intensity of **1′** upon incremental addition of 10 mM Co^{2+} solution in water.

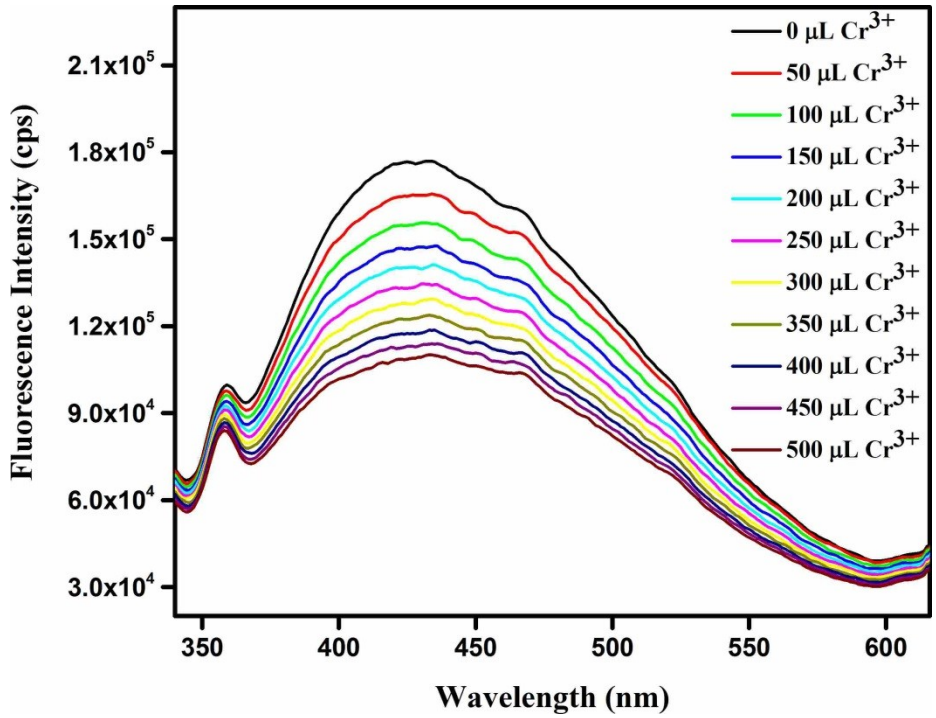

Figure S41. Change in the fluorescence intensity of **1′** upon incremental addition of 10 mM Cr^{3+} solution in water.

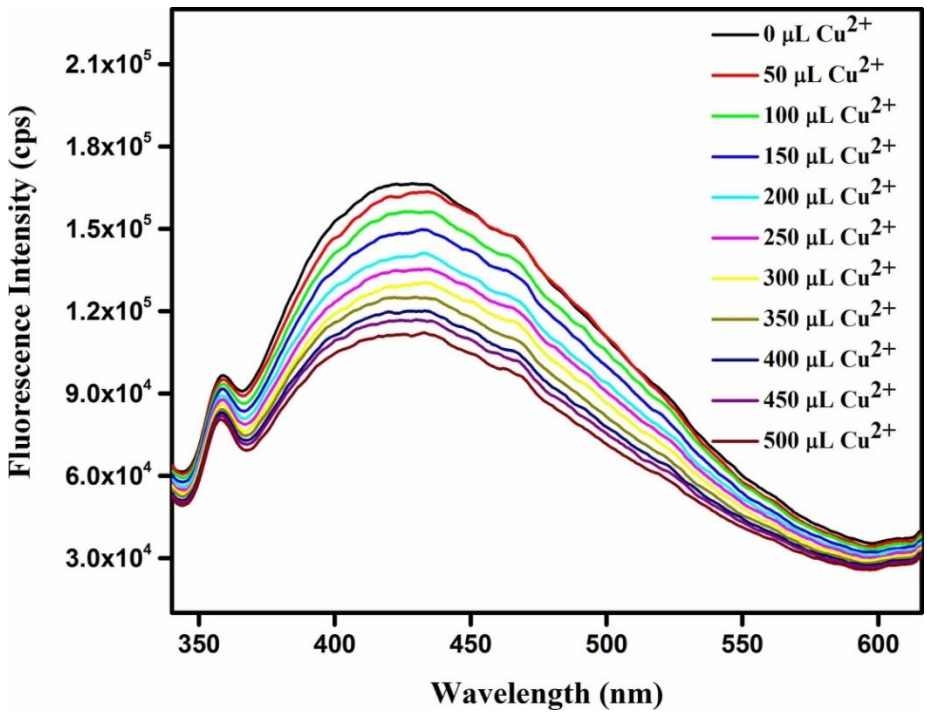

Figure S42. Change in the fluorescence intensity of **1′** upon incremental addition of 10 mM Cu^{2+} solution in water.

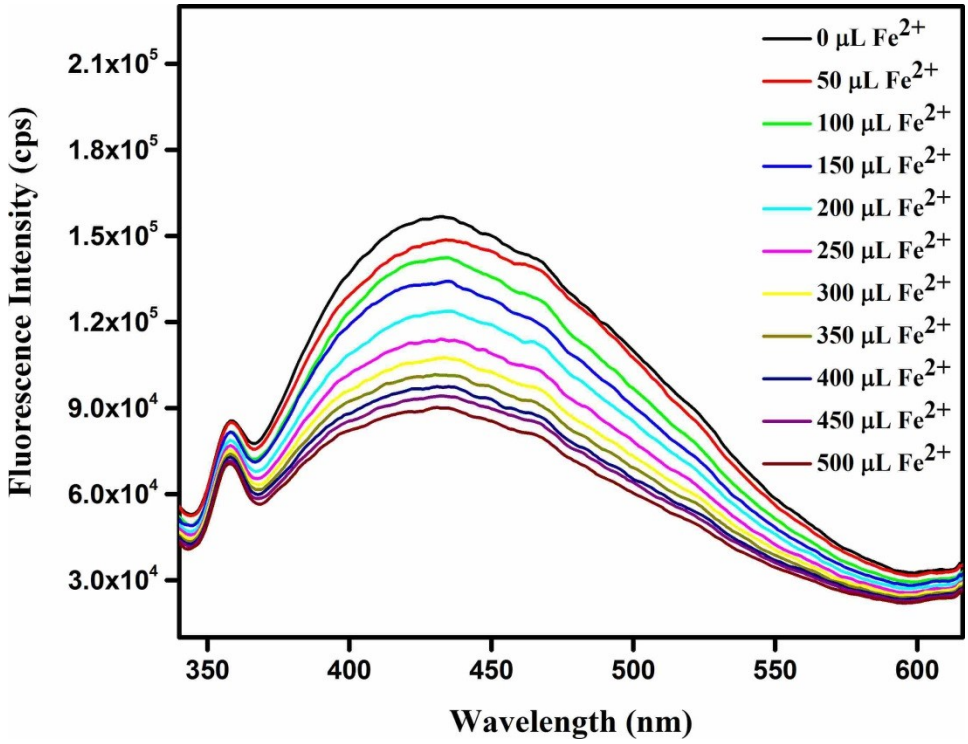

Figure S43. Change in the fluorescence intensity of **1′** upon incremental addition of 10 mM Fe^{2+} solution in water.

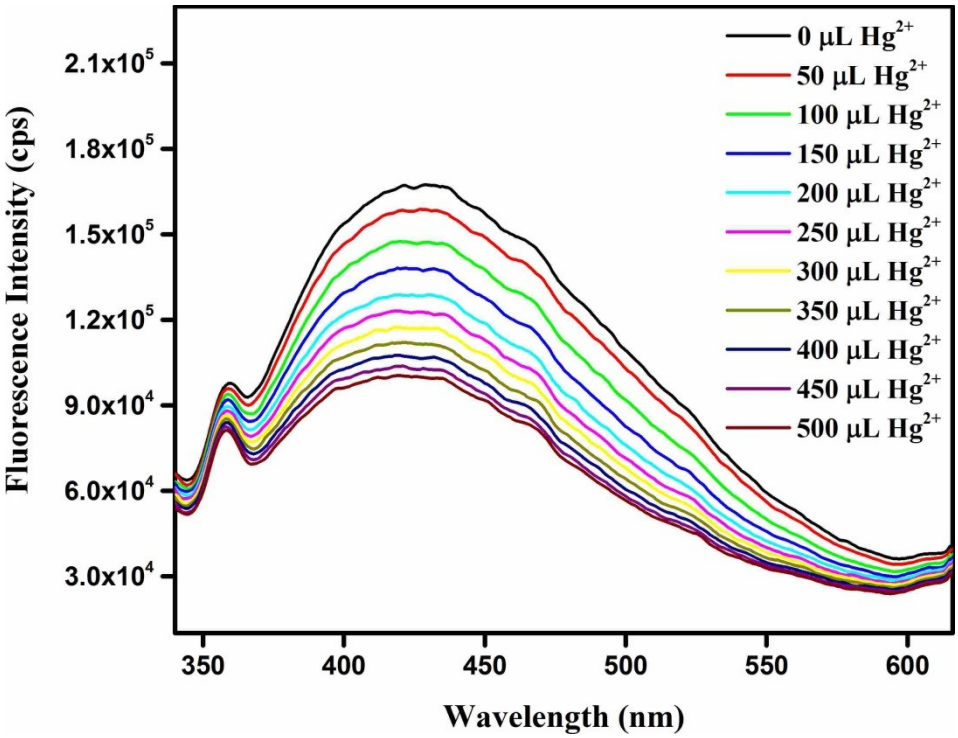

Figure S44. Change in the fluorescence intensity of **1′** upon incremental addition of 10 mM Hg^{2+} solution in water.

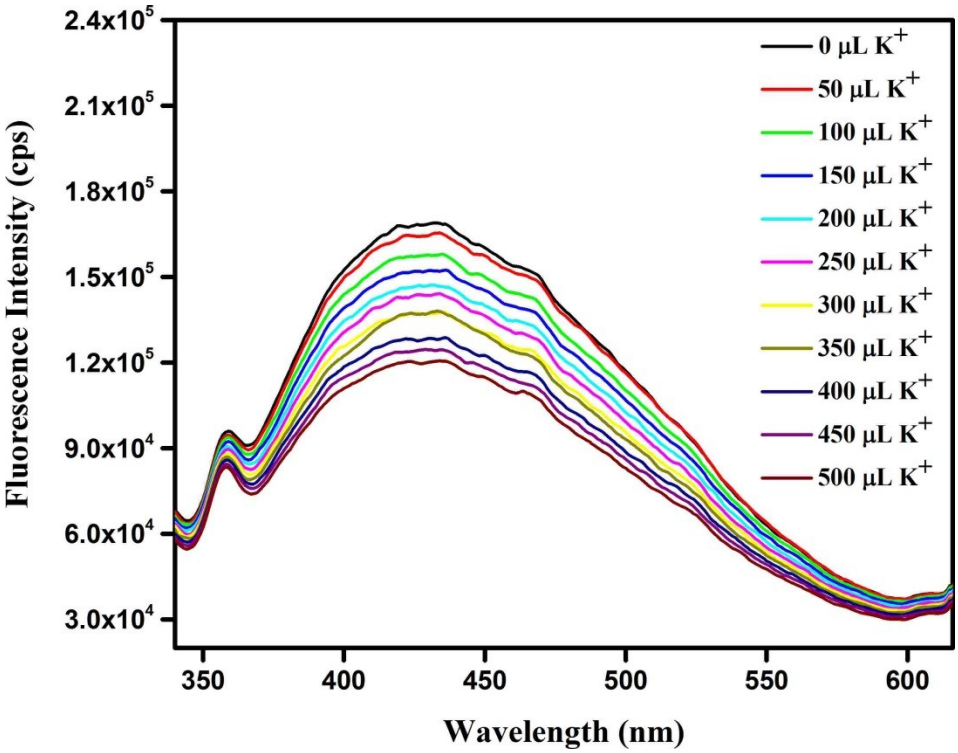

Figure S45. Change in the fluorescence intensity of **1′** upon incremental addition of 10 mM K^{+} solution in water.

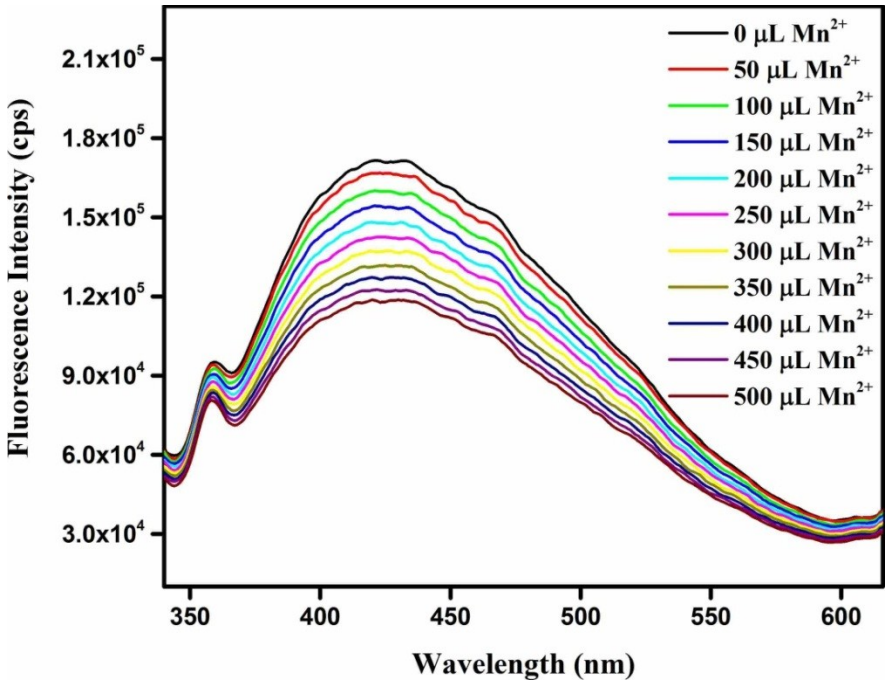

Figure S46. Change in the fluorescence intensity of **1′** upon incremental addition of 10 mM Mn^{2+} solution in water.

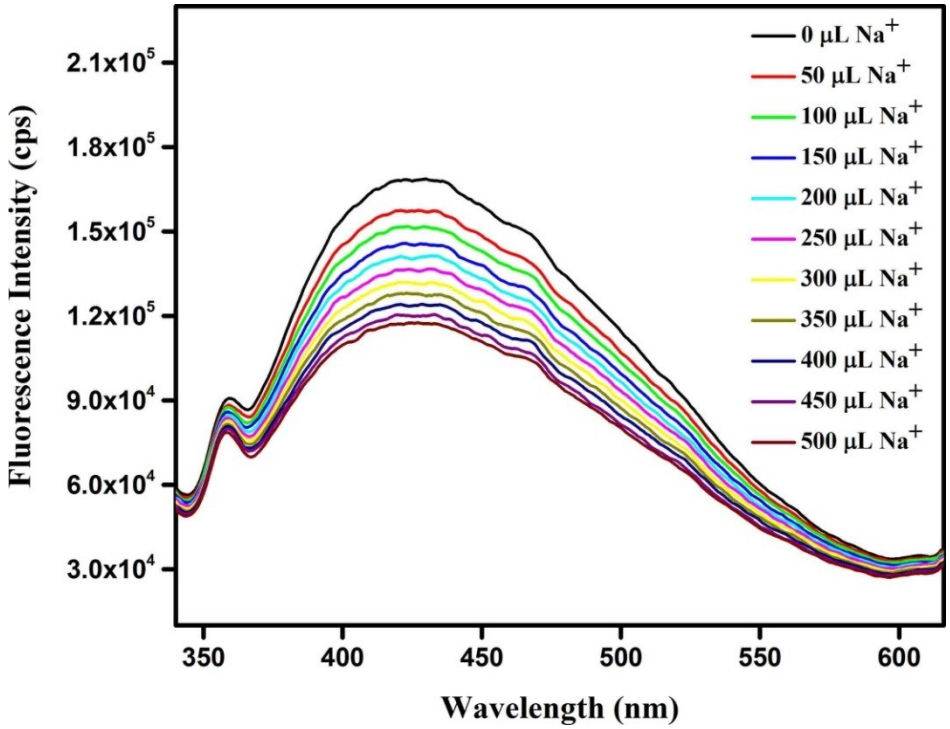

Figure S47. Change in the fluorescence intensity of **1′** upon incremental addition of 10 mM Na^{+} solution in water.

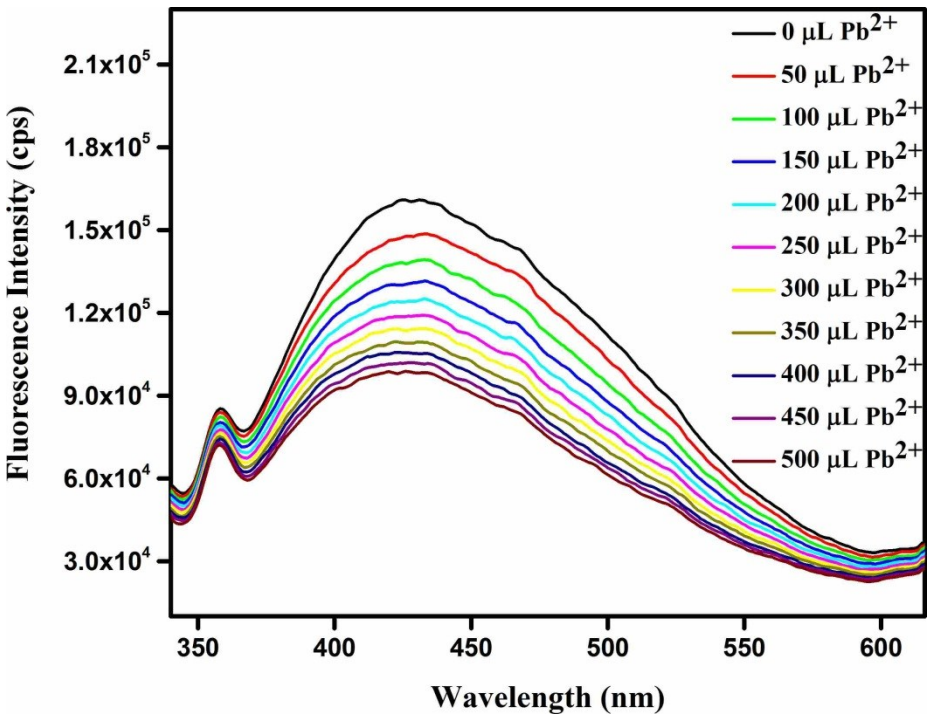

Figure S48. Change in the fluorescence intensity of **1′** upon incremental addition of 10 mM Pb^{2+} solution in water.

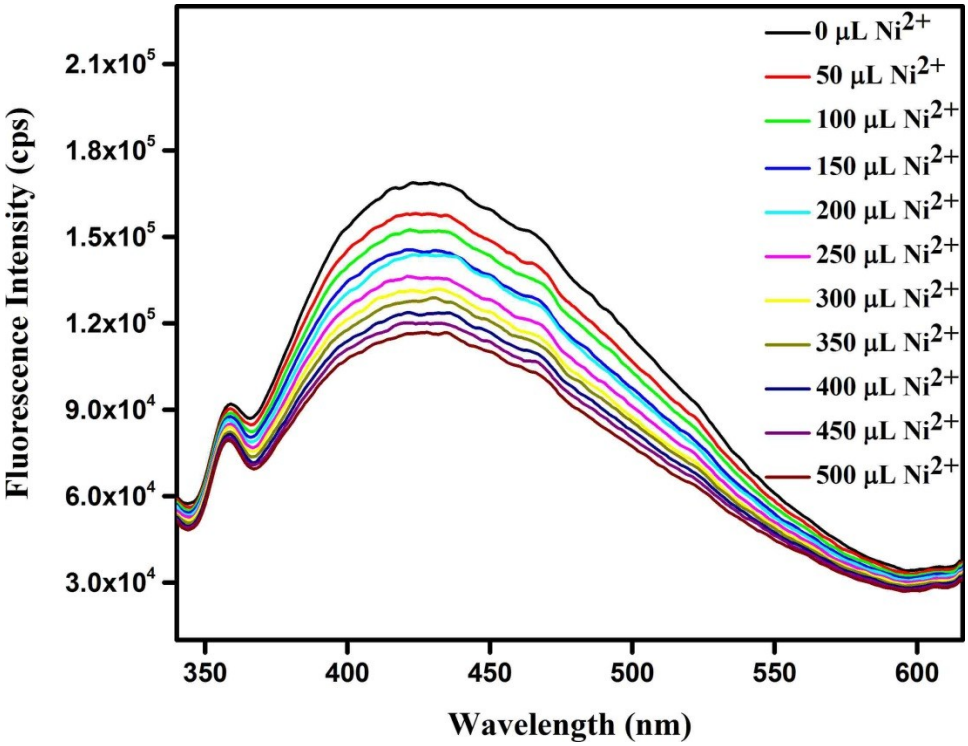

Figure S49. Change in the fluorescence intensity of **1′** upon incremental addition of 10 mM Ni^{2+} solution in water.

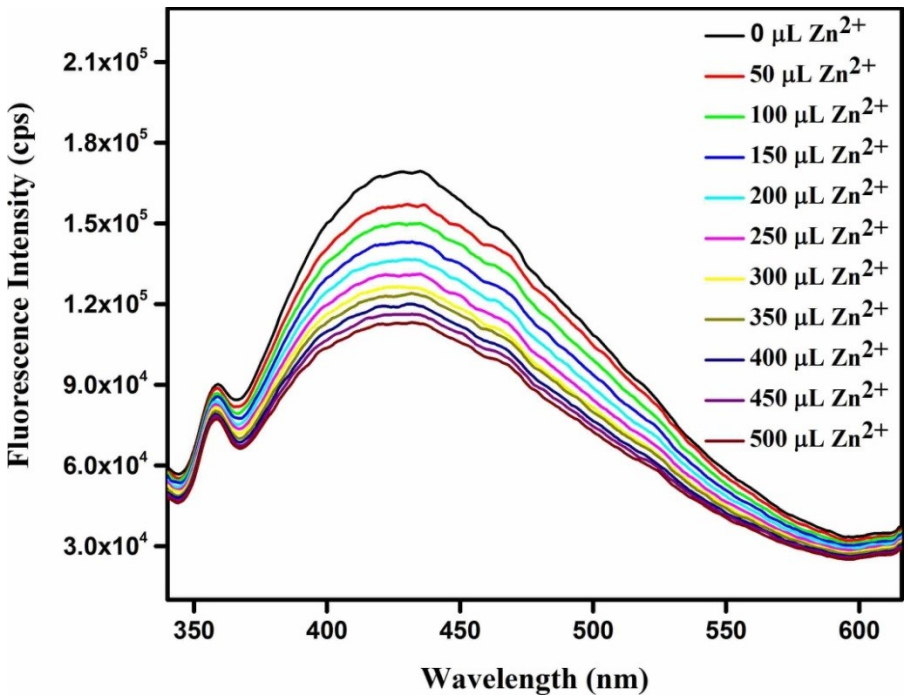

Figure S50. Change in the fluorescence intensity of **1′** upon incremental addition of 10 mM Zn^{2+} solution in water.

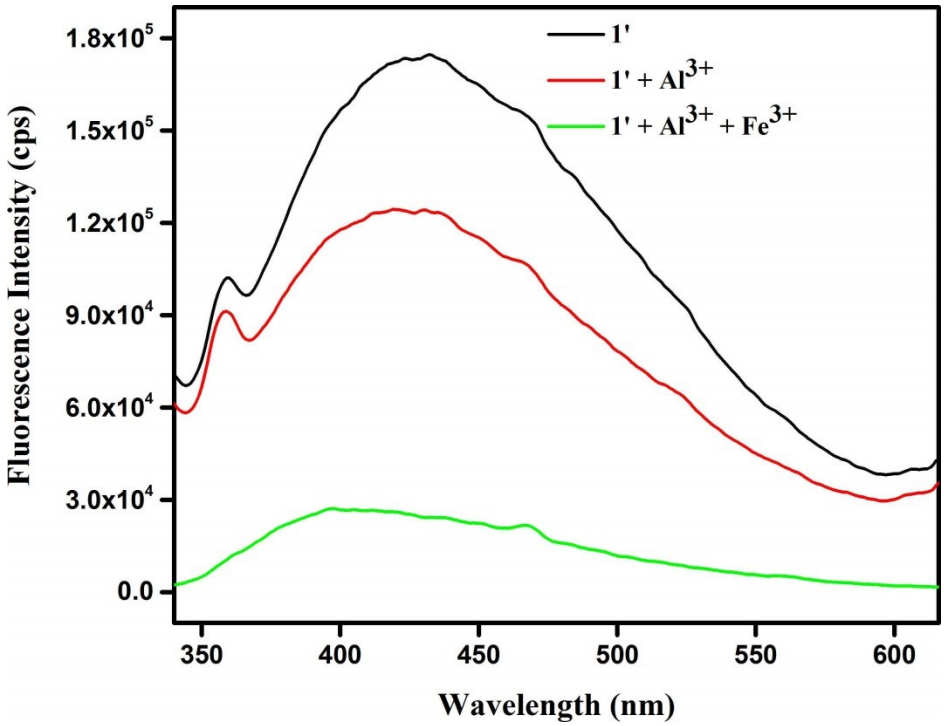

Figure S51. Change in the fluorescence intensity of **1′** upon addition of 10 mM Al^{3+} solution (500 μL) in presence of 10 mM Fe^{3+} (500 μL) solution in water.

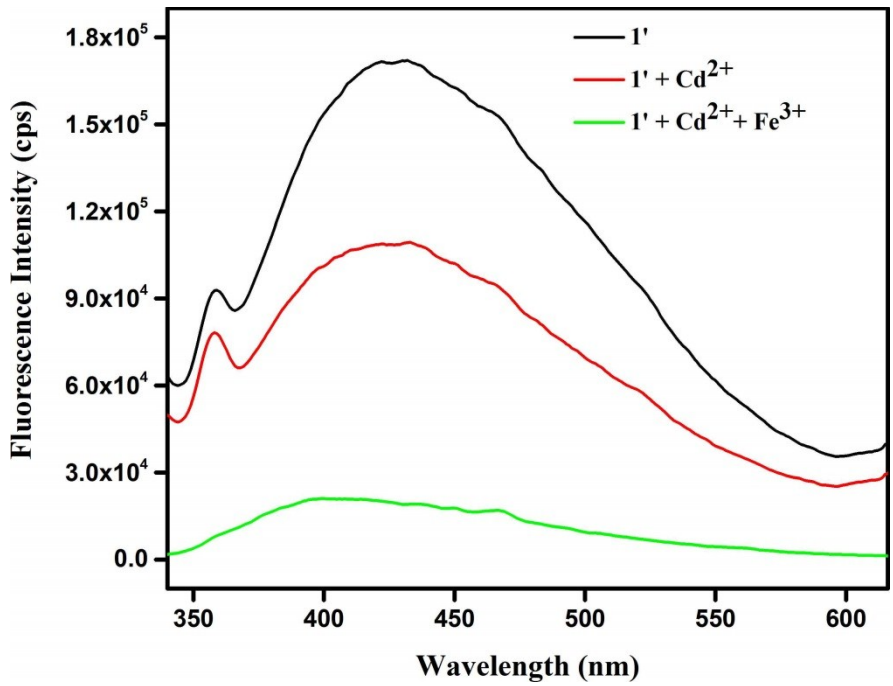

Figure S52. Change in the fluorescence intensity of **1′** upon addition of 10 mM Cd^{2+} solution (500 µL) in presence of 10 mM Fe^{3+} (500 µL) solution in water.

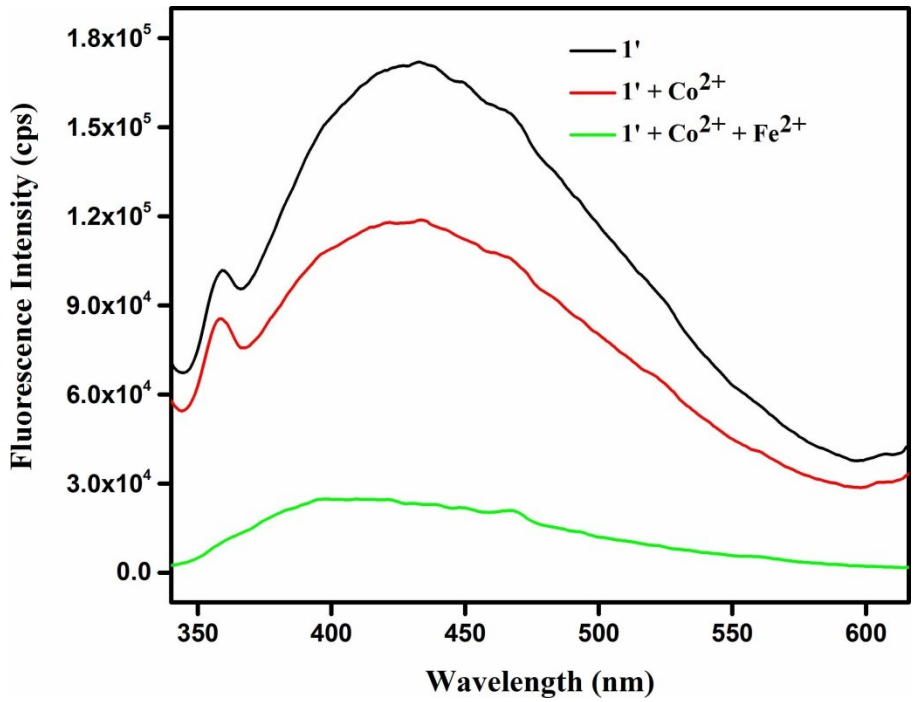

Figure S53. Change in the fluorescence intensity of **1′** upon addition of 10 mM Co^{2+} solution (500 µL) in presence of 10 mM Fe^{3+} (500 µL) solution in water.

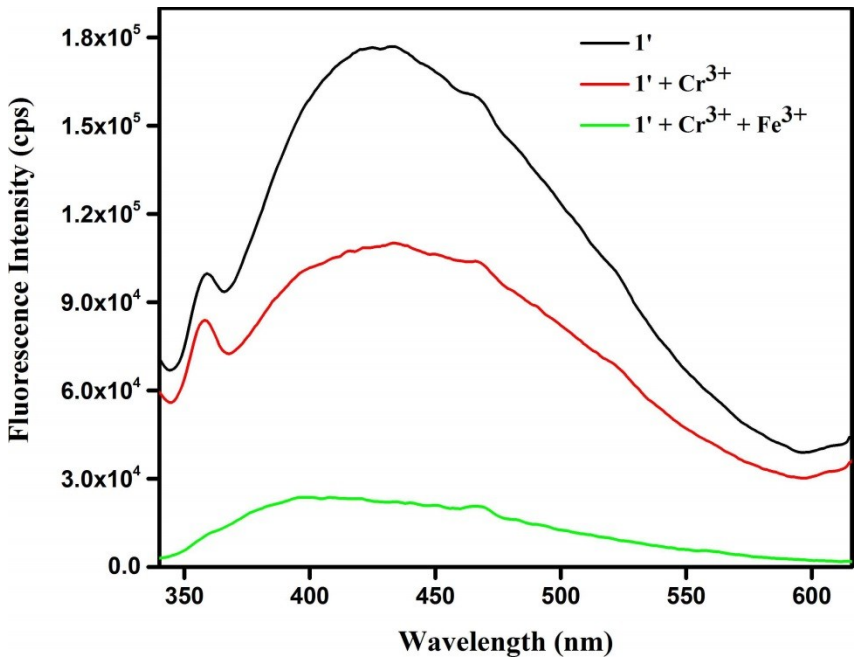

Figure S54. Change in the fluorescence intensity of **1′** upon addition of 10 mM Cr^{3+} solution (500 μL) in presence of 10 mM Fe^{3+} (500 μL) solution in water.

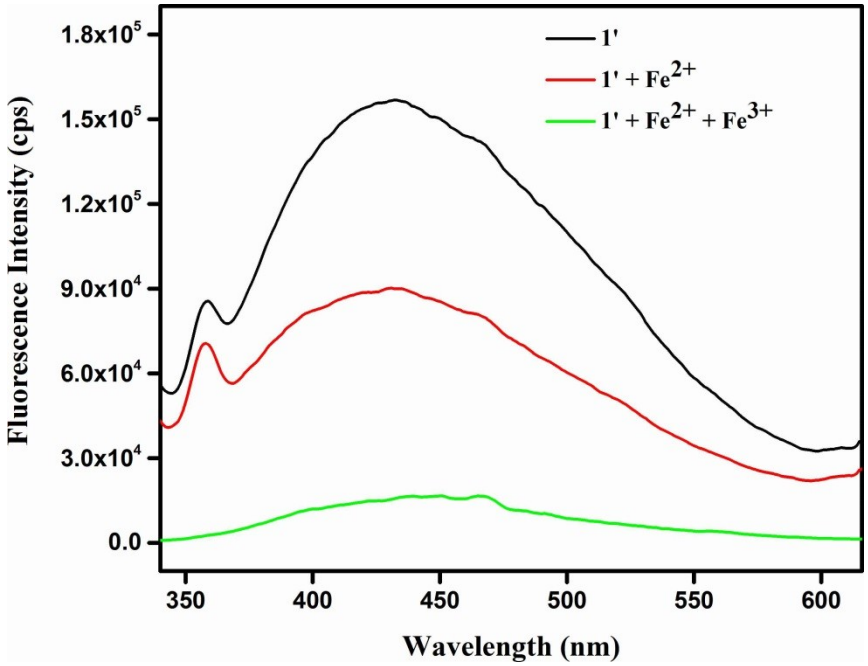

Figure S55. Change in the fluorescence intensity of **1′** upon addition of 10 mM Fe^{2+} solution (500 μL) in presence of 10 mM Fe^{3+} (500 μL) solution in water.

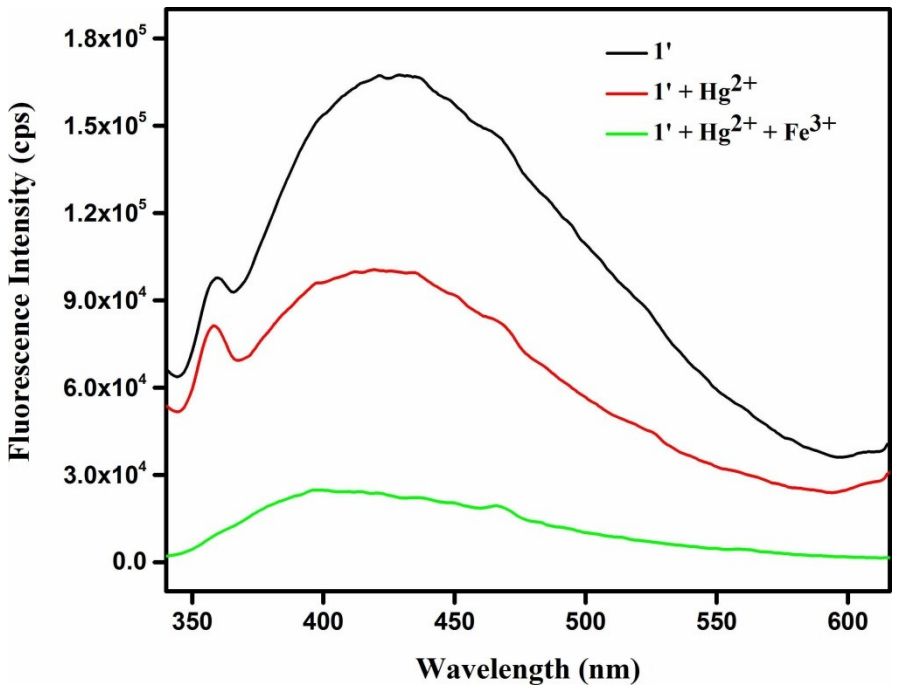

Figure S56. Change in the fluorescence intensity of **1′** upon addition of 10 mM Hg^{2+} solution (500 μL) in presence of 10 mM Fe^{3+} (500 μL) solution in water.

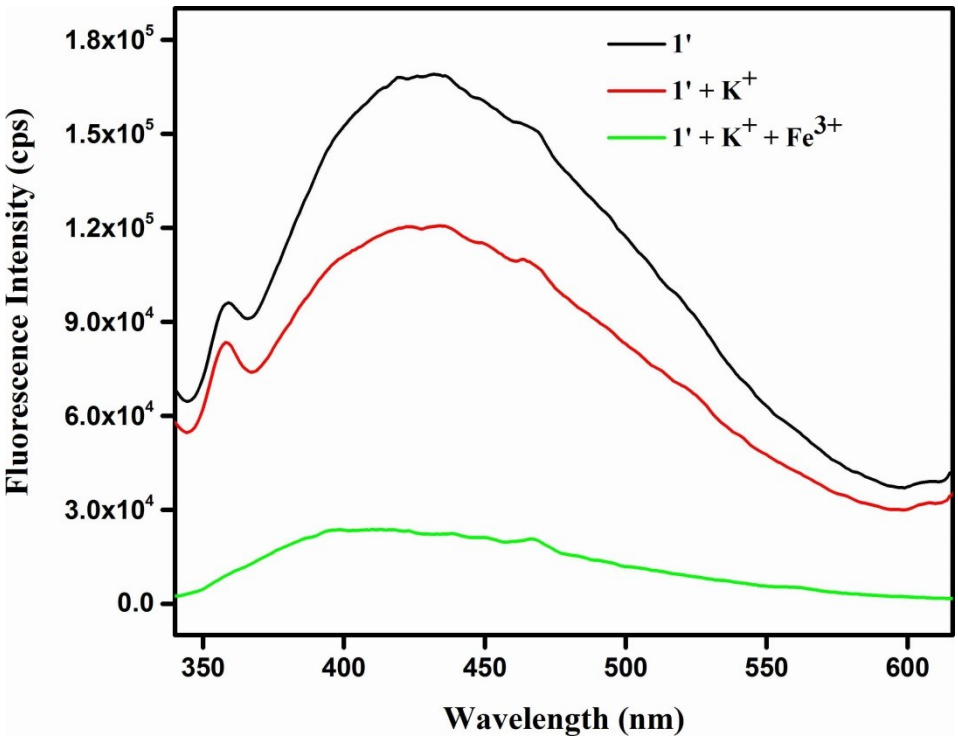

Figure S57. Change in the fluorescence intensity of **1′** upon addition of 10 mM K^{+} solution (500 μL) in presence of 10 mM Fe^{3+} (500 μL) solution in water.

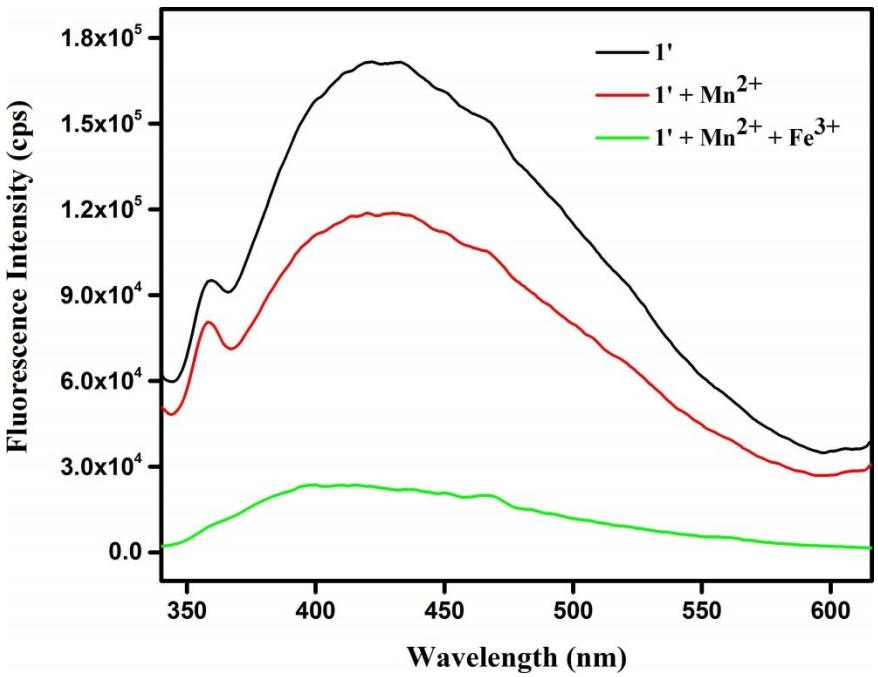

Figure S58. Change in the fluorescence intensity of **1′** upon addition of 10 mM Mn^{2+} solution (500 μL) in presence of 10 mM Fe^{3+} (500 μL) solution in water.

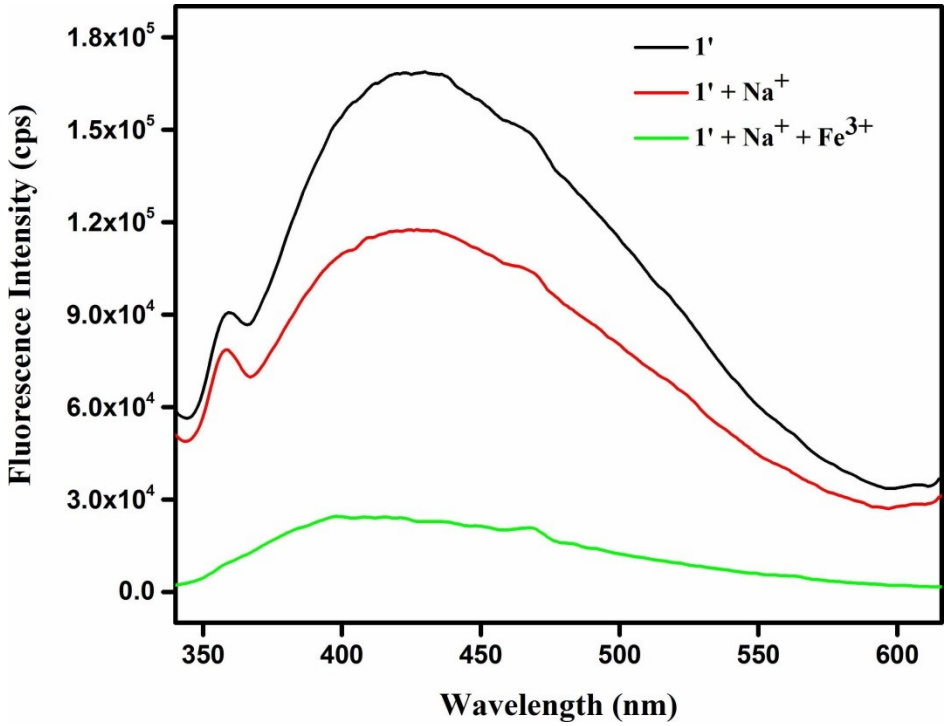

Figure S59. Change in the fluorescence intensity of **1′** upon addition of 10 mM Na^{+} solution (500 μL) in presence of 10 mM Fe^{3+} (500 μL) solution in water.

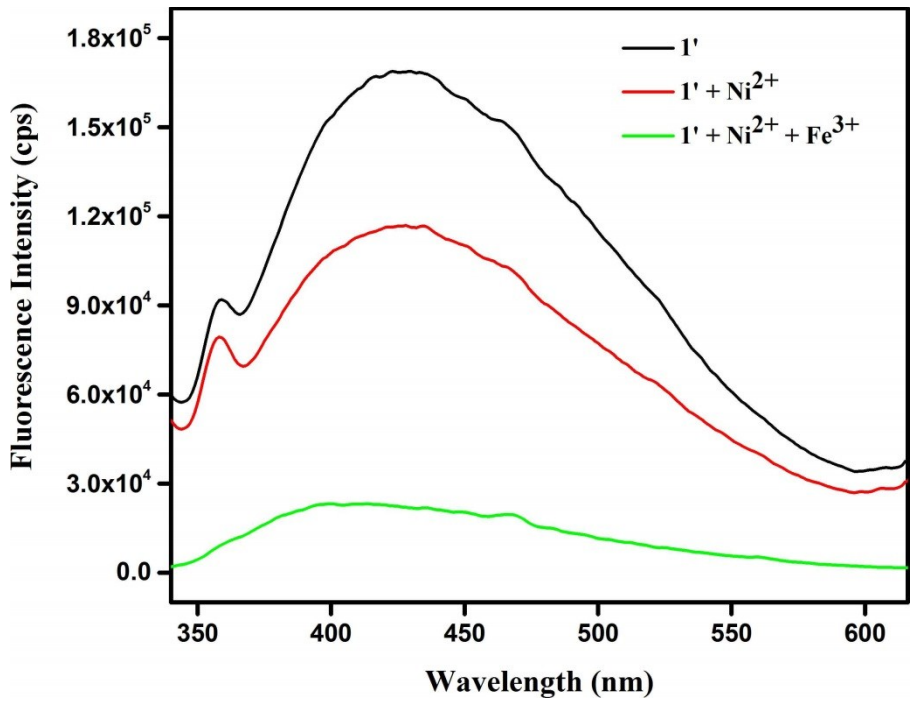

Figure S60. Change in the fluorescence intensity of **1′** upon addition of 10 mM Ni^{2+} solution (500 μL) in presence of 10 mM Fe^{3+} (500 μL) solution in water.

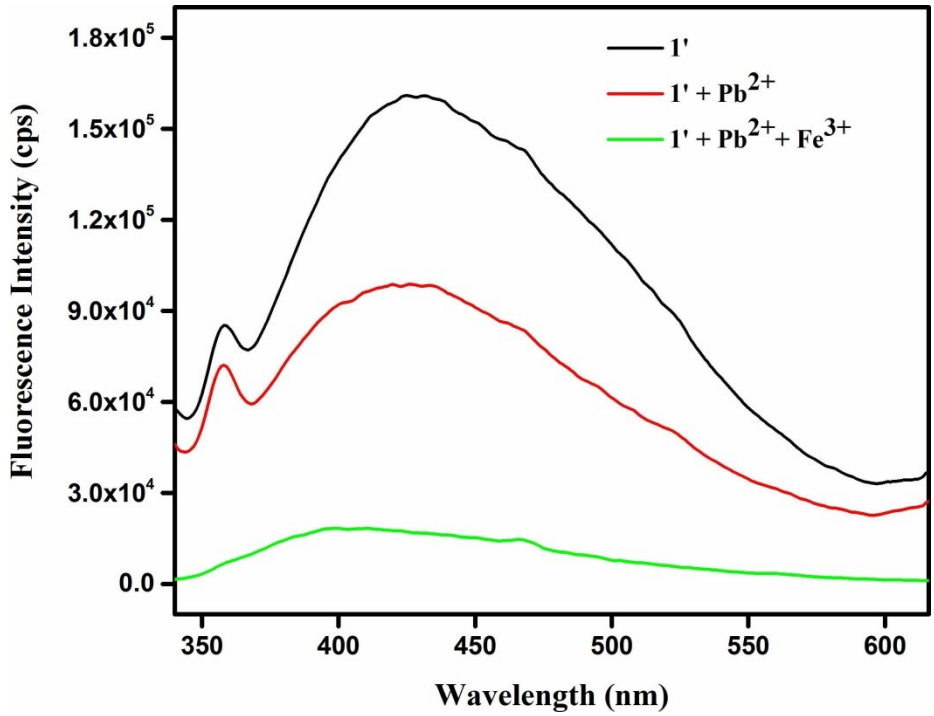

Figure S61. Change in the fluorescence intensity of **1′** upon addition of 10 mM Pb^{2+} solution (500 μL) in presence of 10 mM Fe^{3+} (500 μL) solution in water.

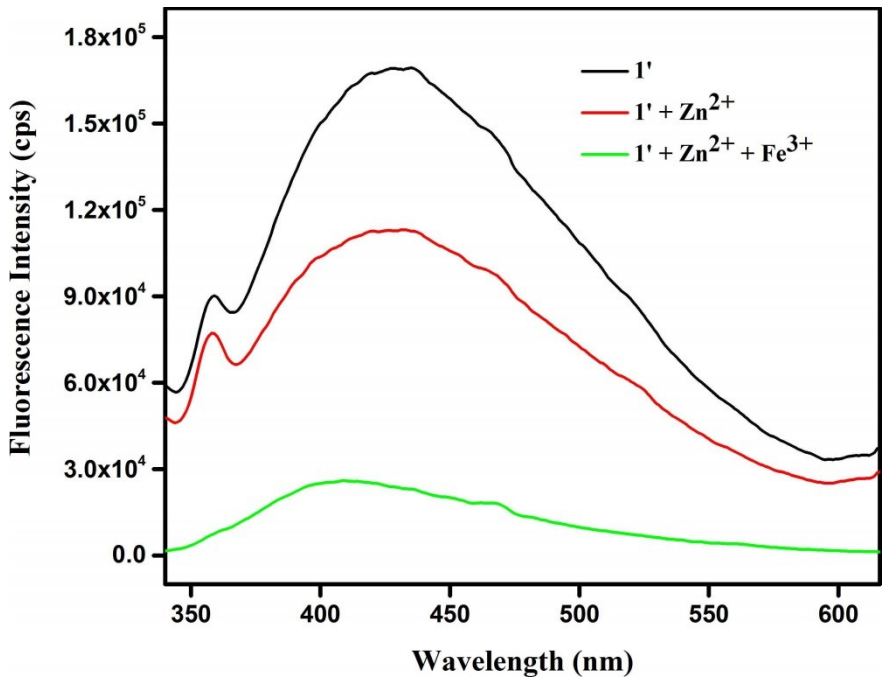

Figure S62. Change in the fluorescence intensity of **1′** upon addition of 10 mM Zn^{2+} solution (500 μL) in presence of 10 mM Fe^{3+} (500 μL) solution in water.

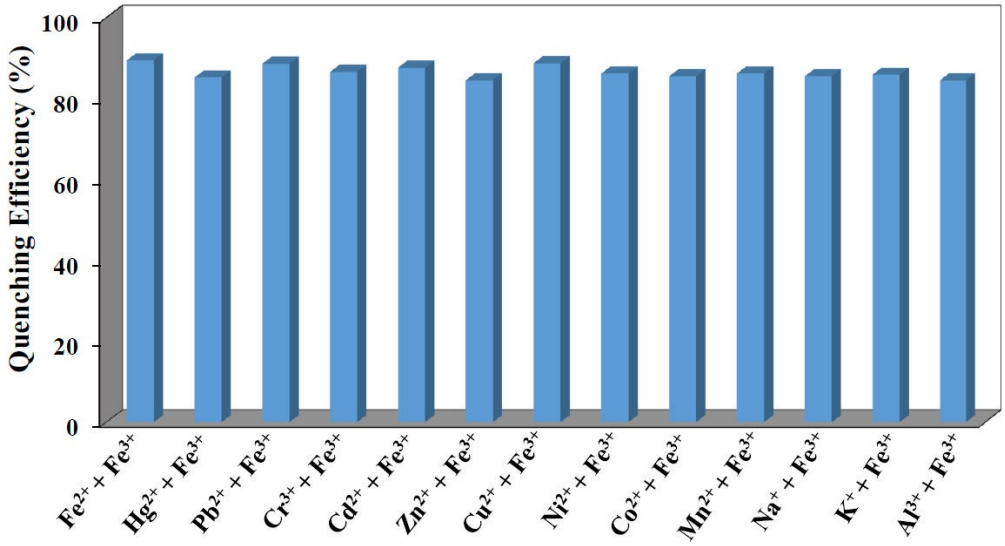

Figure S63. Effect of other metal cations on the quenching efficiency of Fe^{3+} ion in water.

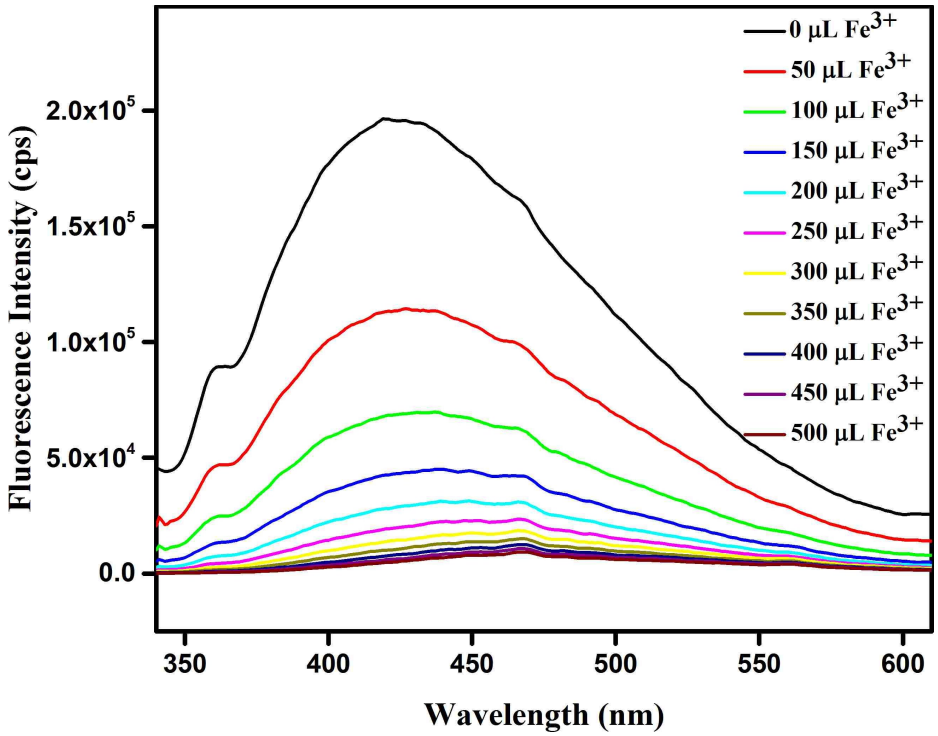

Figure S64. Change in the fluorescence intensity of **1′** in HEPES buffer (10 mM, pH = 7.4) upon incremental addition of 10 mM Fe^{3+} solution.

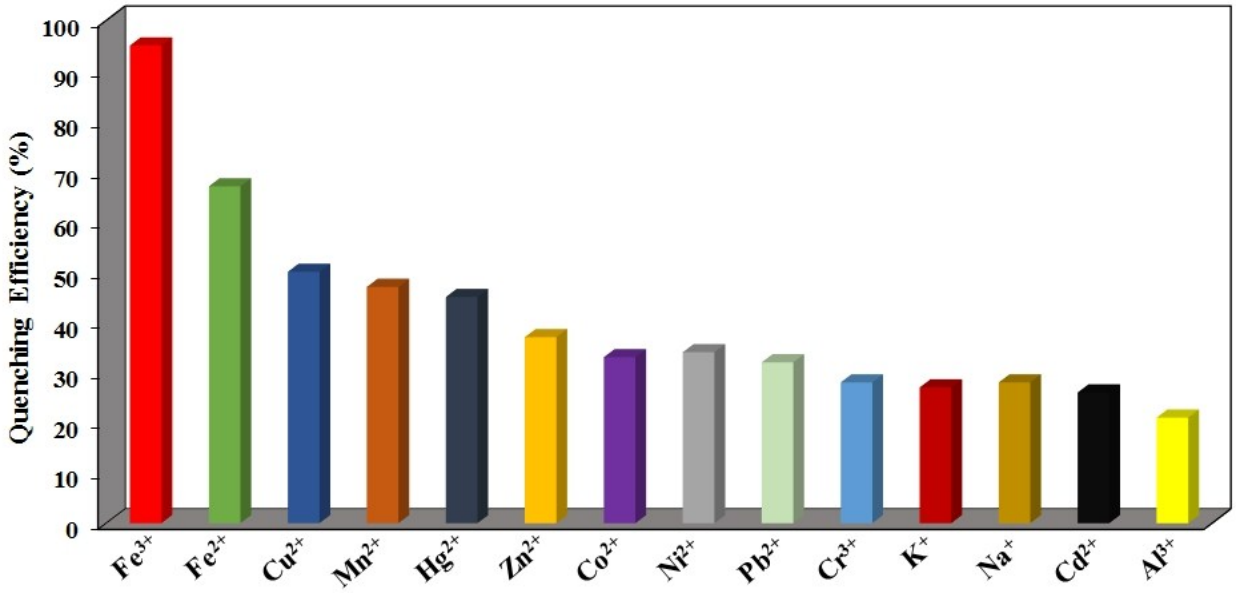

Figure S65. The fluorescence quenching efficiencies of various metal cations (500 μL of 10 mM solution) towards **1'** suspended in HEPES buffer (10 mM, pH = 7.4).

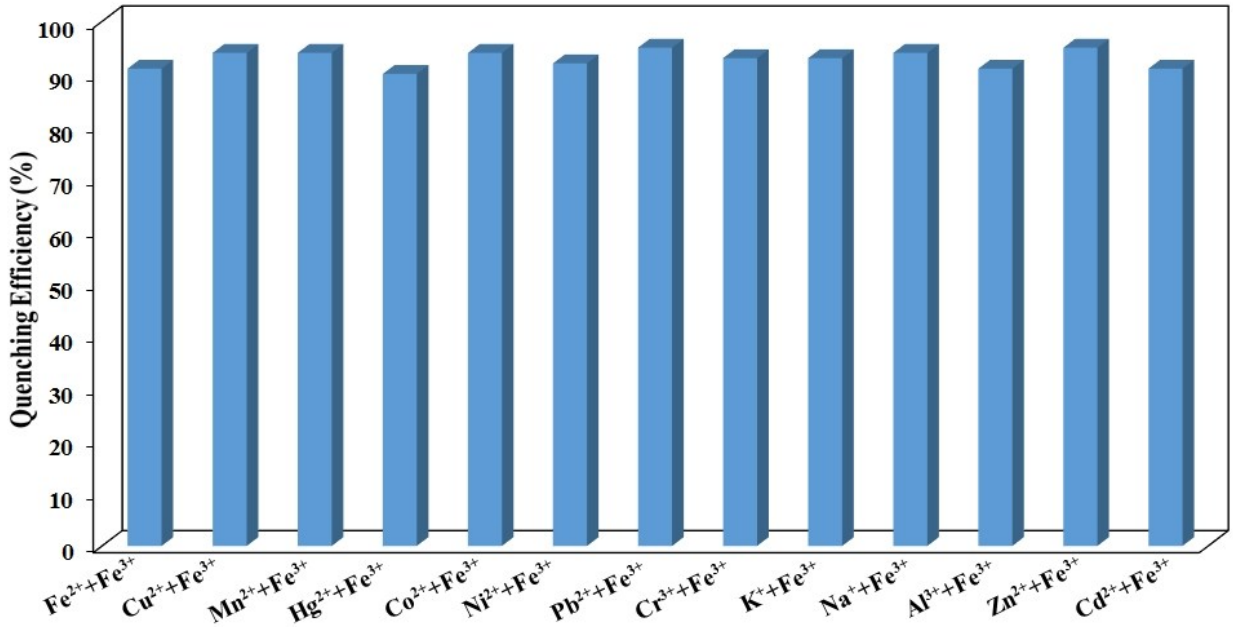

Figure S66. Effect of other metal cations on the quenching efficiency of Fe^{3+} ion in HEPES buffer (10 mM, pH = 7.4).

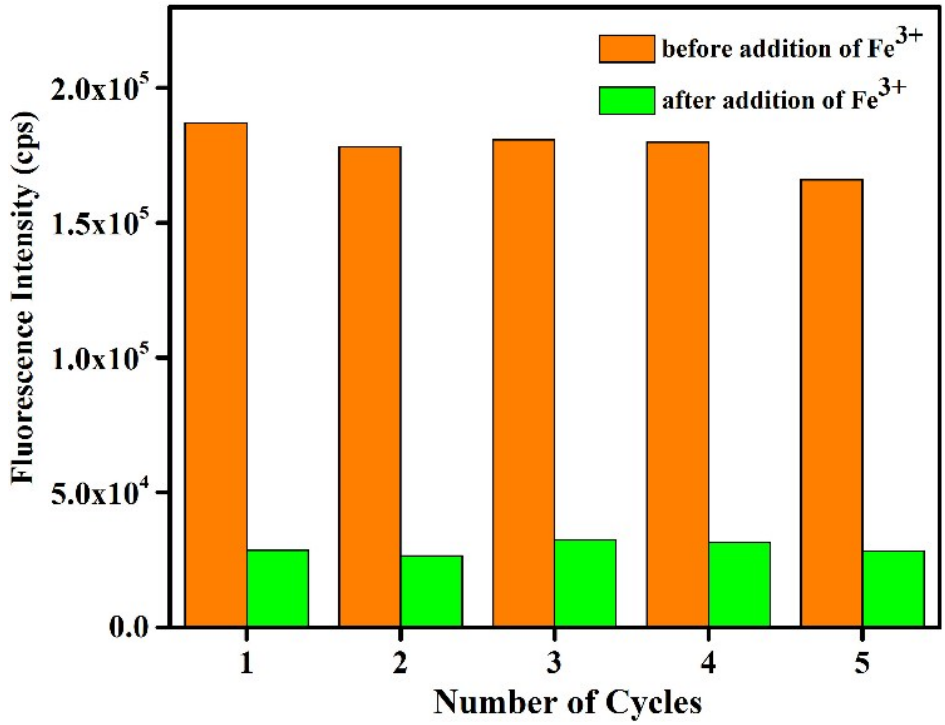

Figure S67. Reproducibility test for the aqueous suspension of **1'** towards sensing of Fe^{3+} ion.

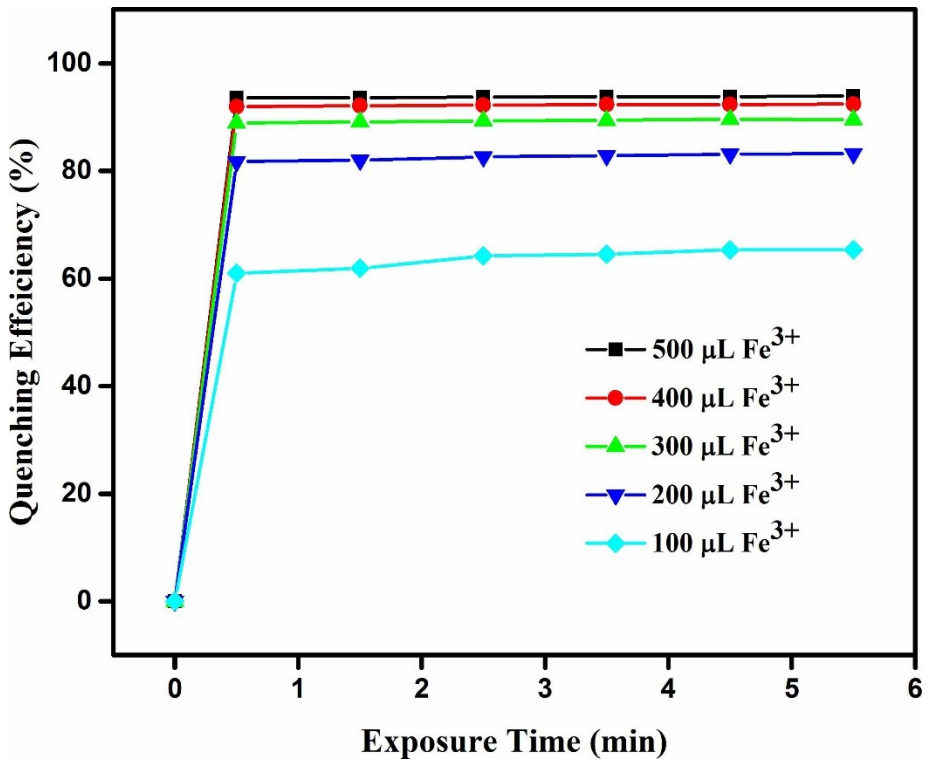

Figure S68. Quenching efficiencies of **1'**as a function of exposure time in water.

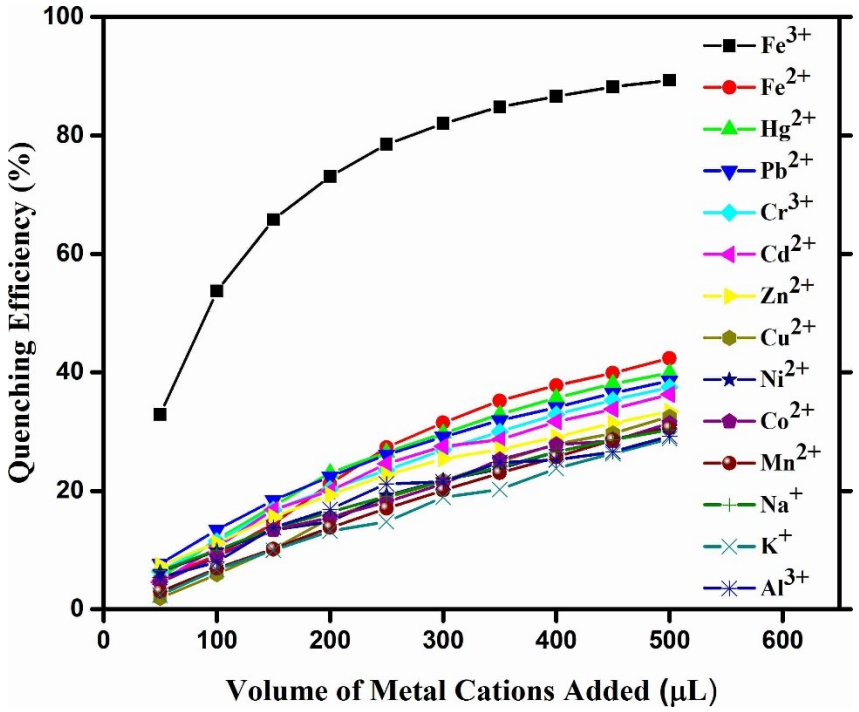

Figure S69. Change of fluorescence quenching efficiencies upon gradual addition of 10 mM solution of various metal cations to a 3 mL well-dispersed suspension of **1′** in water.

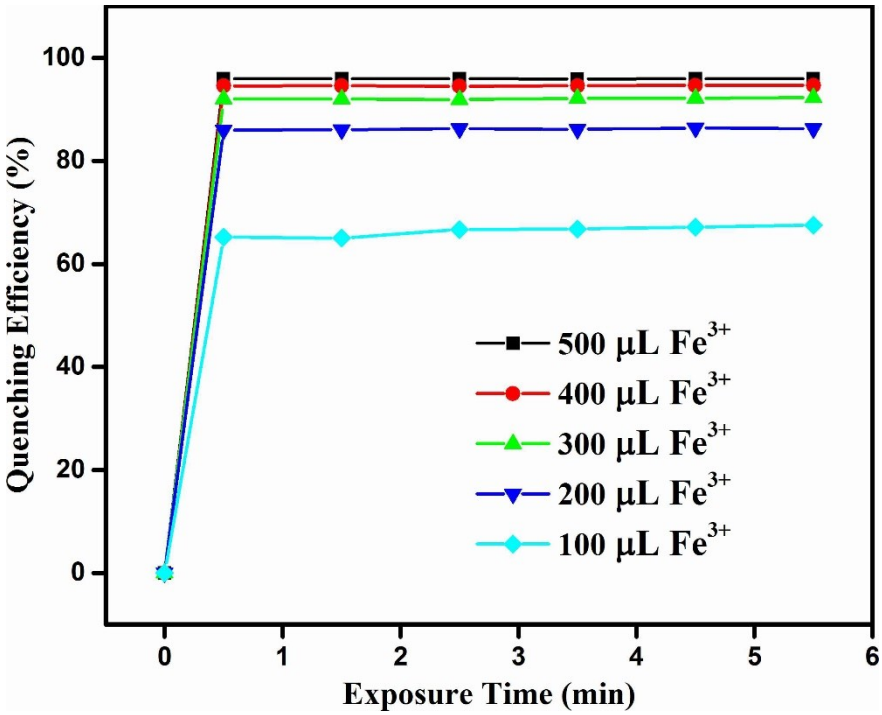

Figure S70. Quenching efficiencies of **1'** in HEPES buffer (10 mM, pH = 7.4) as a function of exposure time.

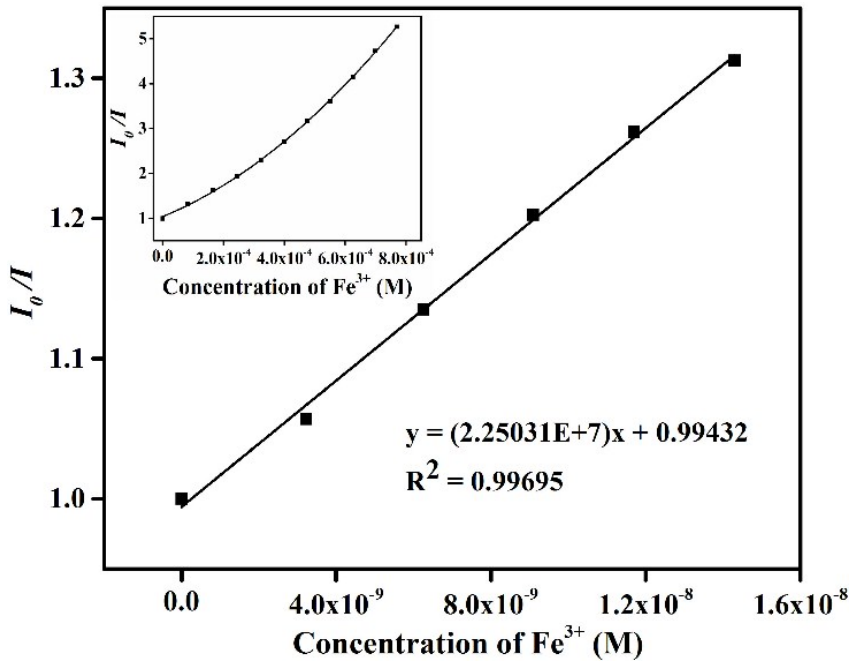

Figure S71. Stern-Volmer plot for the quenching of **1'** at lower concentrations of Fe^{3+} ion in water. Inset: non linearity of the Stern-Volmer plot at higher concentrations of Fe^{3+} ion.

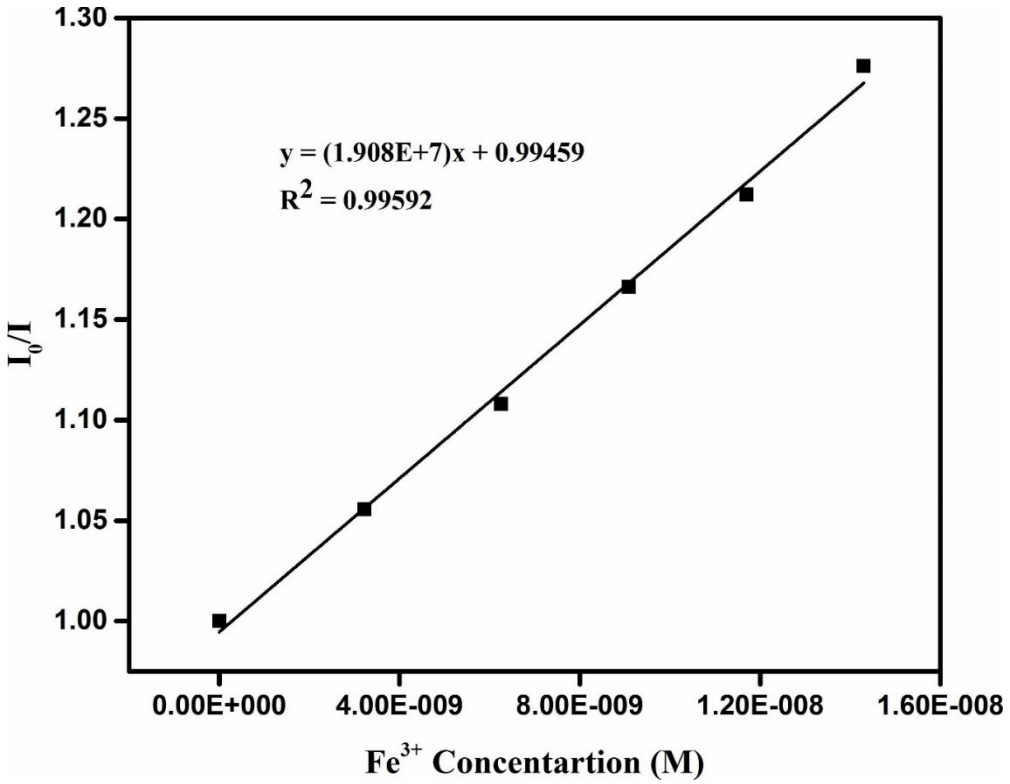

Figure S72. Stern-Volmer plot for the quenching of **1'** at lower concentrations of Fe^{3+} ion in HEPES buffer (10 mM, pH=7.4).

Table S5. A comparison of the Stern-Volmer constant (K_{sv}), detection limit and medium used for Fe^{3+} detection for MOFs reported till date.

Sl. No.	MOF	K_{sv} (M^{-1})	Detection Limit	Medium Used	Ref.
1.	$[Zr_6O_6(OH)_2(CF_3COO)_2(C_{11}H_5NO_4)_4(H_2O)_4]$	2.25×10^7	1.7×10^{-9} M	Water	This work
2.	$[Zr_6O_6(OH)_2(CF_3COO)_2(C_{11}H_5NO_4)_4(H_2O)_4]$	1.91×10^7	2.7×10^{-9} M	HEPES buffer	This work
3.	$[La(TPT)(DMSO)_2]\cdot H_2O$	1.36×10^4	-	ethanol	9
4.	$[H(H_2O)_8][DyZn_4(imdc)_4(im)_4]$	2.88×10^4	-	DMSO	10
5.	EuL_3	4.1×10^3	10^{-4} M	ethanol	11
6.	$[Eu_2(MFDA)_2(HCOO)_2(H_2O)_6]\cdot H_2O$	-	3.3×10^{-7} M	DMF	12
7.	$[Cd(H_2L_a)_{0.5}(H_2L_b)_{0.5}(H_2O)]$	-	10^{-5} M	water	13
8.	$[(CH_3)_2NH_2]\cdot[Tb(bptc)]\cdot x$solvents	-	72.76 ppm	ethanol	14
9.	$[Ln_2(Ccbp)_3\cdot 6H_2O]\cdot 3Cl^-\cdot 4H_2O$	1.143×10^5	-	ethanol	15
10.	Eu^{3+}@MIL-124	3.87×10^4	0.28×10^{-6} M	water	16
11.	MIL-53(Al)	-	0.9×10^{-6} M	PBS buffer	17
12.	$[Ln(Hpzbc)_2(NO_3)]\cdot H_2O$	-	2.6×10^{-5} M	ethanol	18
13.	$[Tb(BTB)(DMF)]\cdot 1.5DMF\cdot 2.5H_2O$	-	10^{-5} M	ethanol	19

14.	$[Tb_4(OH)_4(DSOA)_2(H_2O)_8]\cdot(H_2O)_8$	3.5×10^4	-	water	20
15.	Tb^{3+}@Cd-MOF	1.108×10^5	0.010 mM	DMF	21
16.	$[Zr_6O_4(OH)_4(2,7\text{-CDC})_6]\cdot 19H_2O\cdot 2DMF$	5.5×10^3	9.10×10^{-7} M	water	1

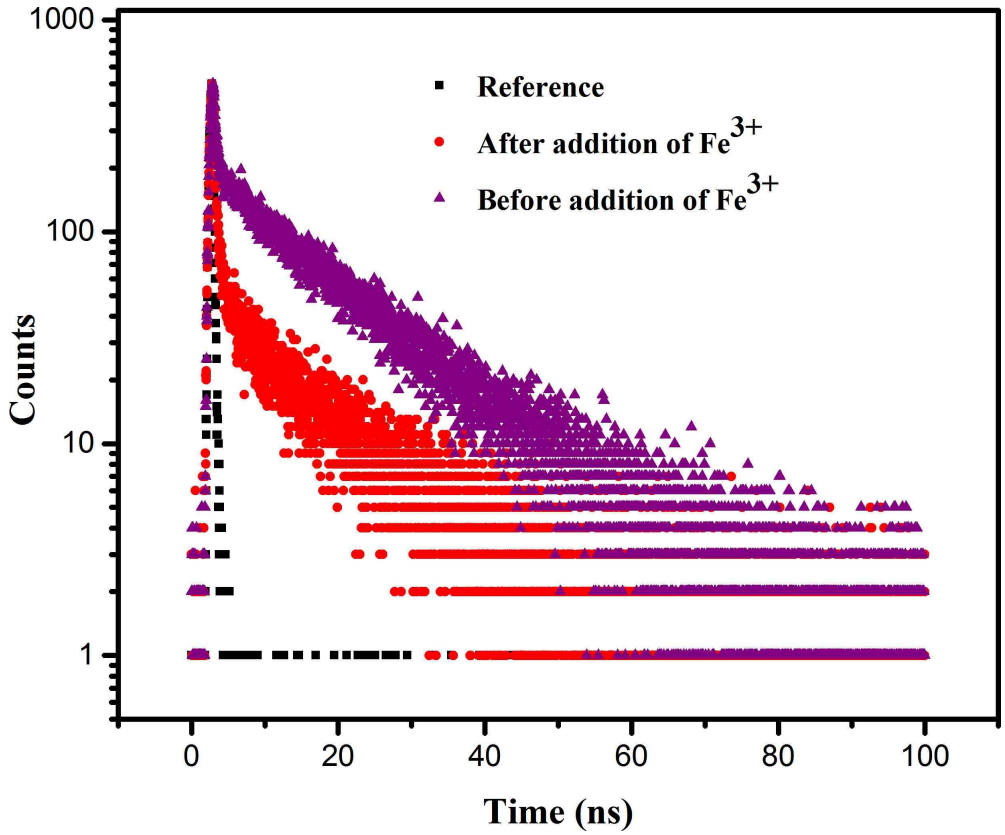

Figure S73. Lifetime decay profile of **1′** before and after addition of 200 μL of 10 mM Fe^{3+} solution in water.

Table S6. Average excited state lifetime (<τ>) values of **1'** before and after addition of 300 μL of 10 mM Fe^{3+} solution (λ_{ex} = 330 nm).

Volume of Fe^{3+} solution added (μL)	B_1	B_2	a_1	a_2	τ_1 (ns)	τ_2 (ns)	<τ>* (ns)	χ^2
0	0.068	0.014	0.10	0.90	0.35	14.68	13.20	1.09
300	0.144	0.002	0.69	0.31	0.22	7.99	2.60	0.92

* $\langle\tau\rangle = a_1\tau_1 + a_2\tau_2$

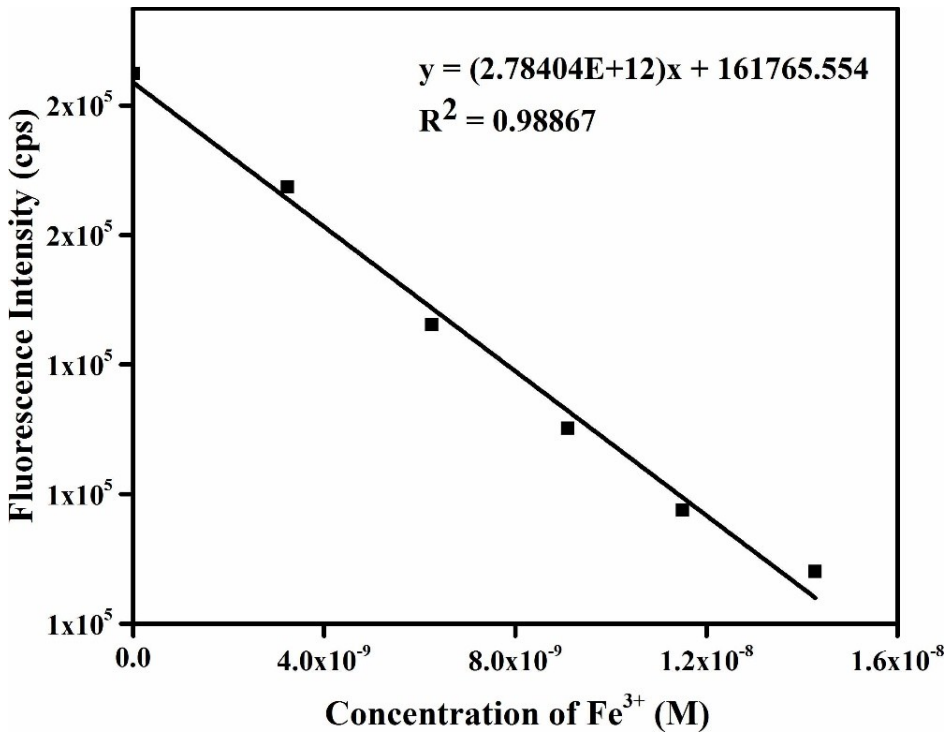

Figure S74. Fluorescence intensity of **1'** in water as a function of Fe^{3+} concentration.

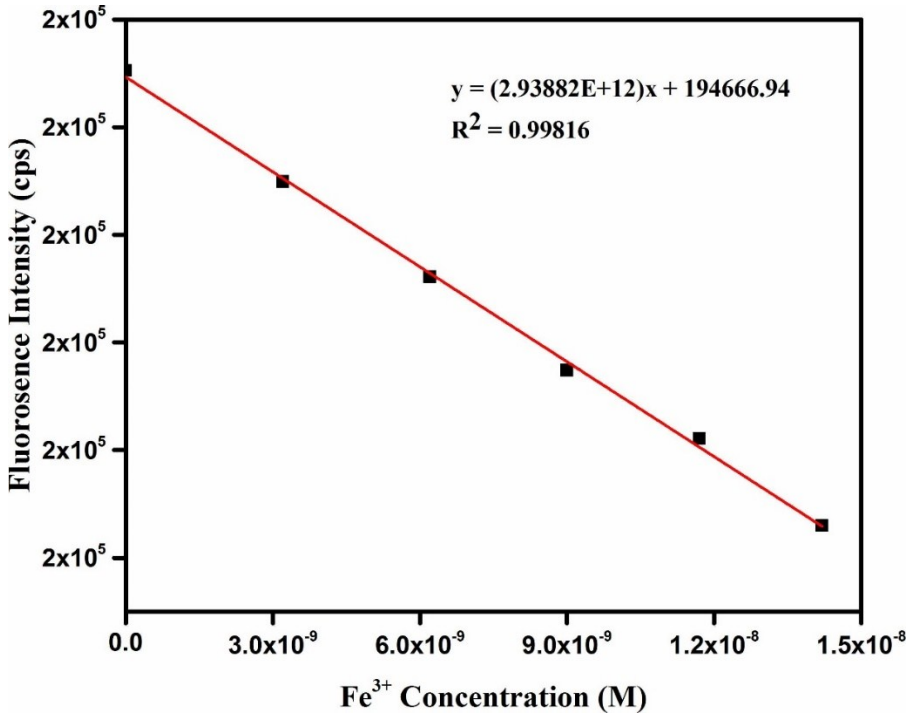

Figure 75. Fluorescence intensity of **1'** in HEPES buffer (10 mM, pH = 7.4) as a function of Fe^{3+} concentration.

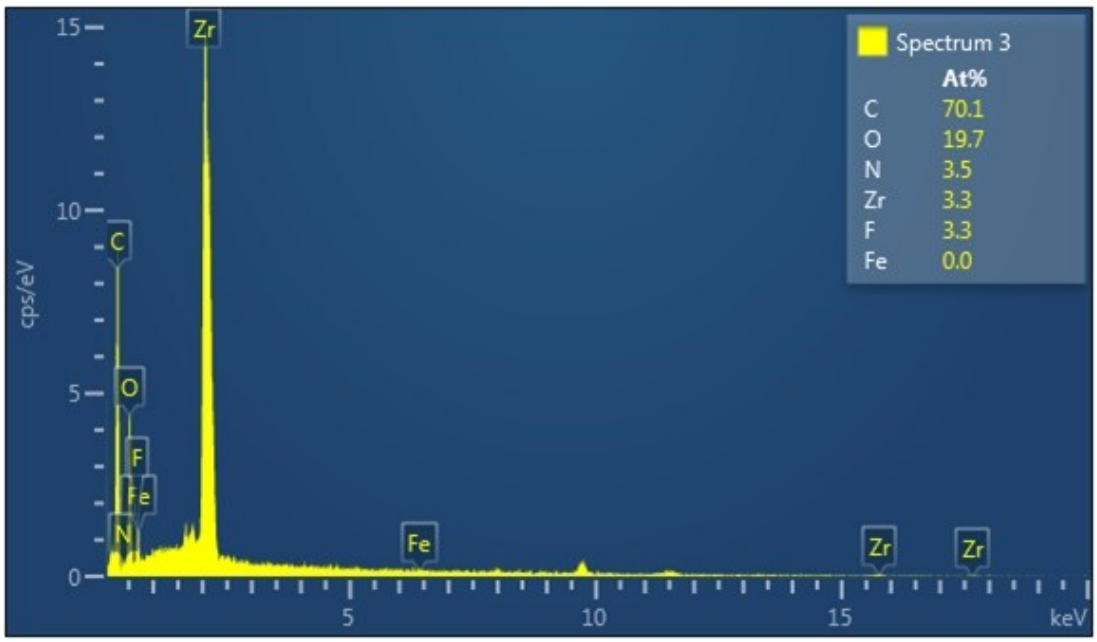

Figure S76. EDX spectrum of **1′** after treatment with 10 mM Fe^{3+} aqueous solution.

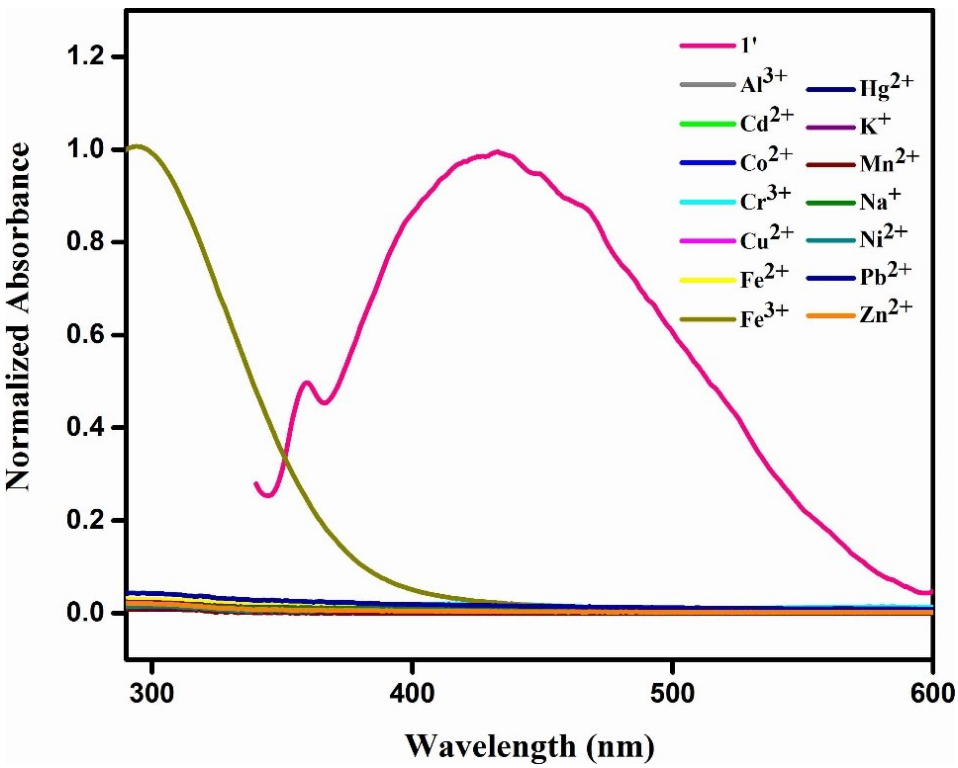

Figure S77. UV-Vis absorption spectra of the aqueous solutions containing different metal ions (10×10^{-3} M). The emission spectra of **1'** (pink color) (3 mg) dispersed in water (3 mL).

Calculated Crystallographic Information File (CIF) for compound 1:

```
data_compound 1
_chemical_name_mineral ??
_cell_length_a  11.6730(20)
_cell_length_b  17.6881(29)
_cell_length_c  25.4979(34)
_cell_angle_alpha 90
_cell_angle_beta  90
_cell_angle_gamma 90
_cell_volume 5264.6(14)
_symmetry_space_group_name_H-M IMMM
loop_
_symmetry_equiv_pos_as_xyz
      '-x, -y, -z'
      '-x, -y, z'
      '-x, y, -z'
      '-x, y, z'
      'x, -y, -z'
      'x, -y, z'
      'x, y, -z'
      'x, y, z'
      '-x+1/2, -y+1/2, -z+1/2'
      '-x+1/2, -y+1/2, z+1/2'
      '-x+1/2, y+1/2, -z+1/2'
      '-x+1/2, y+1/2, z+1/2'
      'x+1/2, -y+1/2, -z+1/2'
      'x+1/2, -y+1/2, z+1/2'
      'x+1/2, y+1/2, -z+1/2'
      'x+1/2, y+1/2, z+1/2'
loop_
_atom_site_label
_atom_site_type_symbol
_atom_site_symmetry_multiplicity
_atom_site_fract_x
_atom_site_fract_y
_atom_site_fract_z
_atom_site_occupancy
_atom_site_B_iso_or_equiv
Zr1 Zr   0 0 0 0.09509(43) 1 0.80(24)
O1 O   0 0 0.1026(29) 0.0473(14) 1 0.80(66)
O2 O   0 0.1493(37) 0 -0.0465(16) 1 0.80(66)
Zr2 Zr   0 0.15111(89) 0.10628(57) 0 1 0.80(24)
O3 O   0 0.1161(27) 0.2336(27) 0 1 0.80(66)
O4 O   0 0.3480(40) 0.0809(14) 0 1 0.80(66)
O5 O   0 0.2078(13) 0.15107(91) 0.07189(56) 1 0.80(66)
O6 O   0 0.1105(15) 0.0851(11) 0.13729(74) 1 0.80(66)
C1 C   0 0.1754275 0.1349718 0.1177686 1 0.80(90)
C2 C   0 0.2191206 0.1829315 0.1620391 1 0.80(90)
C3 C   0 0.2979756 0.2418603 0.1534018 1 0.80(90)
C4 C   0 0.3336952 0.2890573 0.1947299 1 0.80(90)
```

```
C5 C   0 0.2906671 0.2787477 0.2455273 1 0.80(90)
N6 N   0 0.1762682 0.1728096 0.2134025 0.5 0.80(90)
C6 C   0 0.1762682 0.1728096 0.2134025 0.5 0.80(90)
G1 O   0 0 0.5 0.5978(25) 1.000(71) 2.2(15)
G2 O   0 0.514(18) 0.1117(35) 0.6510(16) 0.500(25) 2.2(15)
G3 O   0 0 0.5 0.3110(23) 1.000(64) 2.2(15)
G4 O   0 0.5562(59) 0.1790(40) 0.4109(20) 0.500(30) 2.2(15)
G5 O   0 0 0.3220(62) 0.4431(35) 0.465(50) 2.2(15)
```

References:

1. A. Das and S. Biswas, *Sens. Actuator B-Chem*, 2017, **250**, 121-131.
2. M. Zhang, L. Zhang, Z. Xiao, Q. Zhang, R. Wang, F. Dai and D. Sun, *Sci. Rep.*, 2016, **6**, 20672-20681.
3. R. Wang, X. Liu, A. Huang, W. Wang, Z. Xiao, L. Zhang, F. Dai and D. Sun, *Inorg. Chem.*, 2016, **55**, 1782−1787.
4. X. Wang, L. Zhang, J. Yang, F. Liu, F. Dai, R. Wanga and D. Sun, *J. Mater. Chem. A*, 2015, **3**, 12777–12785.
5. B. Wang, X.-L. Lv, D. Feng, L.-H. Xie, J. Zhang, M. Li, Y. Xie, J.-R. Li and H.-C. Zhou, *J. Am. Chem. Soc*, 2016, **138**, 6204−6216.
6. Q.-H. Tan, Y.-Q. Wang, X.-Y. Guo, H.-T. Liu and Z.-L. Liu, *RSC Adv.*, 2016, **6**, 61725–61731.
7. Y.-Q. Wang, Q.-H. Tan, H.-T. Liu, W-Sun and Z.-L. Liu, *RSC Adv.*, 2015, **5**, 86614-86619.
8. X.-P. Wang, L.-L. Han, Z. Wang, L.-Y. Guo and D. Sun, *J. Mol. Struct.*, 2016, **1107**, 1-6.
9. C. Zhang, Y. Yan, Q. Pan, L. Sun, H. He, Y. Liu, Z. Liang and J. Li, *Dalton Trans.*, 2015, **44**, 13340–13346.
10. Y.-F. Li, D. Wang, Z. Liao, Y. Kang, W.-H. Ding, X.-J. Zheng and L.-P. Jin, *J. Mater. Chem. C*, 2016, **4**, 4211-4217.
11. M. Zheng, H. Tan, Z. Xie, L. Zhang, X. Jing and Z. Sun, *ACS Appl. Mater. Interfaces*, 2013, **5**, 1078−1083.
12. X.-H. Zhou, L. Li, H.-H. Li, A. Li, T. Yanga and W. Huang, *Dalton Trans.*, 2013, **42**, 12403–12409.
13. Y. Wu, G.-P. Yang, Y. Zhang, N. Shi, J. Han and Y.-Y. Wang, *RSC Adv.*, 2015, **5**, 90772-90777.
14. X.-L. Zhao, D. Tian, Q. Gao, H.-W. Sun, J. Xu and X.-H. Bu, *Dalton Trans.*, 2016, **45**, 1040–1046.
15. K.-M. Wang, L. Du, Y.-L. Ma, J.-S. Zhao, Q. Wang, T. Yan and Q.-H. Zhao, *CrystEngComm*, 2016, **18**, 2690–2700.
16. X.-Y. Xu and B. Yan, *ACS Appl. Mater. Interfaces*, 2014, **7**, 721-729.
17. C.-X. Yang, H.-B. Ren and X.-P. Yan, *Anal. Chem.*, 2013, **85**, 7441−7446.
18. G.-P. Li, G. Liu, Y.-Z. Li, L. Hou, Y.-Y. Wang and Z. Zhu, *Inorg. Chem.*, 2016, **55**, 3952-3959.
19. H. Xu, H.-C. Hu, C.-S. Cao and B. Zhao, *Inorg. Chem.*, 2015, **54**, 4585−4587.

20. X.-Y. Dong, R. Wang, J.-Z. Wang, S.-Q. Zang and T. C. W. Mak, *J. Mater. Chem. A*, 2015, **3**, 641–647.
21. H. Weng and B. Yan, *Sens. Actuator B-Chem.*, 2016, **228**, 702–708.

22. Frisch, M. J.; Trucks, G. W.; Schlegel, H. B.; Scuseria, G. E.; Robb, M. A.; Cheeseman, J. R.; Scalmani, G.; Barone, V.; Mennucci, B.; Petersson, G. A.; Nakatsuji, H.; Caricato, M.; Li, X.; Hratchian, H. P.; Izmaylov, A. F.; Bloino, J.; Zheng, G.; Sonnenberg, J. L.; Hada, M.; Ehara, M.; Toyota, K.; Fukuda, R.; Hasegawa, J.; Ishida, M.; Nakajima, T.; Honda, Y.; Kitao, O.; Nakai, H.; Vreven, T.; J. A. Montgomery, J.; Peralta, J. E.; Ogliaro, F.; Bearpark, M.; Heyd, J. J.; Brothers, E.; Kudin, K. N.; Staroverov, V. N.; Kobayashi, R.; Normand, J.; Raghavachari, K.; Rendell, A.; Burant, J. C.; Iyengar, S. S.; Tomasi, J.; Cossi, M.; Rega, N.; Millam, J. M.; Klene, M.; Knox, J. E.; Cross, J. B.; Bakken, V.; Adamo, C.; Jaramillo, J.; Gomperts, R.; Stratmann, R. E.; Yazyev, O.; Austin, A. J.; Cammi, R.; Pomelli, C.; Ochterski, J. W.; Martin, R. L.; Morokuma, K.; Zakrzewski, V. G.; Voth, G. A.; Salvador, P.; Dannenberg, J. J.; Dapprich, S.; Daniels, A. D.; Farkas, O.; Foresman, J. B.; Ortiz, J. V.; Cioslowski, J.; Fox, D. J., *Gaussian 09, Revision A.1*. Gaussian, Inc.: Wallingford CT, ***2009***.